Representation of phosphorus cycle in Joint UK Land Environment Simulator (vn5.5_JULES-CNP)

Mahdi (André) Nakhavali[1], Lina M. Mercado[1,2], Iain P. Hartley[1], Stephen Sitch[1], Fernanda V Cunha[3], Raffaello di Ponzio[3], Laynara F. Lugli[3], Carlos A. Quesada[3], Kelly M. Andersen[1,4,5], Sarah E. Chadburn[6], Andy J. Wiltshire[1,7], Douglas B. Clark[2], Gyovanni Ribeiro[3], Lara Siebert[3], Anna C. M. Moraes[3], Jéssica Schmeisk Rosa[3], Rafael Assis[3] and José L. Camargo[3]

[1]University of Exeter, College of Life and Environmental Sciences, Exeter, EX4 4QE, United Kingdom
[2]UK Centre for Ecology and Hydrology, Wallingford, OX10 8BB, United Kingdom
[3]Coordination of Environmental Dynamics, National Institute of Amazonian Research, Manaus, AM 69060-062, Brazil
[4] University of Edinburgh, School of Geosciences, Edinburgh, EH8 9AB, UK
[5] Nanyang Technological University, Asian School of the Environment, Singapore, 639798, Singapore
[6]College of Engineering, Mathematics, and Physical Sciences, University of Exeter, Exeter, EX4 4QE, United Kingdom
[7]Met Office Hadley Centre, Exeter, Devon, EX1 3PB, United Kingdom

Correspondence to: Mahdi (André) Nakhavali (m.nakhavali@exeter.ac.uk)

Abstract

Most Land Surface Models (LSMs), the land components of Earth system models (ESMs), include representation of nitrogen (N) limitation on ecosystem productivity. However only few of these models have incorporated phosphorus (P) cycling. In tropical ecosystems, this is likely to be important as N tends to be abundant but the availability of rock-derived elements, such as P, can be very low. Thus, without a representation of P cycling, tropical forest response in areas such as Amazonia to rising atmospheric CO_2 conditions remains highly uncertain. In this study, we introduced P dynamics and its interactions with the N and carbon (C) cycles into the Joint UK Land Environment Simulator (JULES). The new model (JULES-CNP) includes the representation of P stocks in vegetation and soil pools, as well as key processes controlling fluxes between these pools. We develop and evaluate JULES-CNP using in situ data collected at a low fertility site in the Central Amazon, with a soil P content representative of 60% of soils across the Amazon basin, to parameterise, calibrate and evaluate JULES-CNP. Novel soil and plant P pool observations are used for parameterisation and calibration and the model is evaluated against C fluxes and stocks, and for those soil P pools not used for parameterisation/calibration. We then evaluate the model at additional P limited test sites across the Amazon, in Panama and Hawaii showing a significant improvement over the C and CN only versions of the model. The model is then applied under elevated CO_2 (600 ppm) at our study site Central Amazon to quantify the impact of P limitation on CO_2 fertilization. We compare our results against current state of the art CNP models using the same methodology that was used in the AmazonFACE model intercomparison study. The model is able to reproduce the observed plant and soil P pools and fluxes used for evaluation under ambient CO_2. We estimate P to limit net primary productivity (NPP) by 24% under current CO_2 and by 46% under elevated CO_2. Under elevated CO_2, biomass in simulations accounting for CNP increase by 10% relative to contemporary CO_2 conditions, although it is 5% lower compared with CN and C-only simulations. Our results highlight the potential for high P limitation and therefore lower CO_2 fertilization capacity in the Amazon forest with low fertility soils.

1. Introduction

Land ecosystems currently take up about 30% of anthropogenic CO_2 emissions (Friedlingstein *et al.*, 2020), thus buffering the anthropogenic increase in atmospheric CO_2. Tropical forests play a major role in the land C cycle, account for about half of global net primary production (NPP)(Schimel *et al.*, 2015), and store the highest above ground carbon among all biomes (Pan *et al.*, 2011; Mitchard, 2018).

The C sink capacity of tropical forests may be constrained by nutrient availability for plant photosynthesis and growth (Vitousek and Howarth, 1991; Elser *et al.*, 2007; LeBauer and Treseder, 2008) via P (Nordin, Högberg and Näsholm, 2001; Shen *et al.*, 2011) and/or N related processes (DeLuca, Keeney and McCarty, 1992; Perakis and Hedin, 2002). Global process-based models of vegetation dynamics and function suggest a continued land C sink in the tropical forests, largely attributed to the CO_2 fertilization effect (Sitch *et al.*, 2008; Schimel, Stephens and Fisher, 2015; Koch, Hubau and Lewis, 2021). However, many of these models typically do not consider P constraints on plant growth (Fleischer *et al.*, 2019), which is likely to be an important limiting nutrient in tropical ecosystems, characterised by old and heavily weathered soils. The importance of nutrient cycling representation in Earth System Models (ESMs), and the lack thereof, was highlighted by Hungate *et al.* (2003) and Zaehle and Dalmonech (2011), showing the significance of nitrogen inclusion in ESMs for generating more realistic estimations of the future evolution of the terrestrial C sink. However, in the Coupled Climate C Cycle Model Inter-comparison Project (C4MIP), none of the participating ESMs included N dynamics (Friedlingstein *et al.*, 2006). Seven years later, for the update in CMIP5 (Anav *et al.*, 2013), three models out of eighteen with N dynamics were included (Bentsen *et al.*, 2013; Long *et al.*, 2013; Ji *et al.*, 2014). Although much progress has been made in the inclusion of an N cycle in ESMs so far, none of the CMIP5 models included P cycling and in the most recent CMIP6, only one model includes P (ACCESSESM1.5 model) (Arora *et al.*, 2020).

The long history of soil development in tropical regions which involves the loss of rock-derived nutrients through weathering and leaching on geologic timescales (Vitousek et al., 1997, 2010) results in highly weathered soils. Soil P is hypothesized to be among the key limiting nutrients to plant growth in tropical forests (Vitousek *et al.*, 1997, 2010; Hou *et al.*, 2020), unlike temperate forest where N is hypothesised to be the main constraint (Aerts and Chapin, 1999; Luo *et al.*, 2004). Low P availability in tropical soils is related to the limited un-weathered parent material or organic compounds as source of P (Walker and Syers, 1976), active sorption (Sanchez, 1977) and high occlusion (Yang and Post, 2011) which further reduce plant available P. Although N limitation can impact the terrestrial C sink response to increasing atmospheric CO_2 by changing plant C fixation capacity (Luo et al., 2004), this can be partially ameliorated over time by input of N into the biosphere via the continuous inputs of N into ecosystems from atmospheric deposition and biological N fixation (Vitousek et al., 2010). P-limitation is pervasive in natural ecosystems (Hou *et al.*, 2020) and the lack of large P inputs into ecosystems, especially those growing on highly weathered soil, may make P limitation a stronger constraint on ecosystem response to elevated CO_2 (eCO_2) than N (Gentile et al., 2012; Sardans, Rivas-Ubach and Peñuelas, 2012). This causes considerable uncertainty in predicting the future of the Amazon forest C sink (Yang *et al.*, 2014).

There is evidence to suggest P limitation on plant productivity in the Amazon forest (Malhi, 2012) where it has been shown that the younger, more fertile west and south-west Amazon soils have higher tree turnover (Phillips et al., 2004; Stephenson and Van Mantgem, 2005) and stem growth rates (Malhi *et al.*, 2004) and lower above ground biomass (Baker *et al.*, 2004; Malhi *et al.*, 2006) compared to their central and eastern counterparts. Total soil P has been found as the best predictor of stem growth (Quesada *et al.*, 2010) and of total NPP (Aragão *et al.*, 2009) across this fertility gradient, and foliar P is positively related to plant photosynthetic capacity (V_{cmax} and J_{cmax}) in these forests (Mercado *et al.*, 2011).

However, modelling studies are unable to reproduce observed spatial patterns of NPP and biomass in the Amazon, one possible reason being the lack of inclusion of soil P constraints on plant productivity and function (Wang, Law and Pak, 2010; Vicca *et al.*, 2012a; Yang *et al.*, 2014). Nevertheless, some modelling studies have focused on improving process and parameter representation using the observational data of spatial variation in woody biomass residence time (Johnson *et al.*, 2016), soil texture and soil P to parameterise the maximum carboxylation capacity (V_{cmax}) (Castanho *et al.*, 2013). Results from these studies successfully represent observed patterns of Amazon forest biomass growth increases with increasing soil fertility. However, the full representation of these interactions and the impact of the soil nutrient availability on biomass productivity is still missing in most of ESMs.

So far, several dynamic global vegetation models have been developed to represent P cycling within the soil (Yang *et al.*, 2013; Haverd *et al.*, 2018) and between plant and soils for tropical forests particularly (Yang *et al.*,

2014; Zhu *et al.*, 2016; Goll *et al.*, 2017). Furthermore, a comprehensive study included several models with C-N-P cycling and their feedbacks on the atmospheric C fixation and biomass growth in Amazon forests under ambient and elevated CO_2 conditions (eCO$_2$) (Fleischer *et al.*, 2019). Despite these developments, data to underpin them and their projections, particularly for the tropics, is sparse and remains challenging particularly for the Amazon forest (Reed *et al.*, 2015; Jiang *et al.*, 2019). Moreover, due to the lack of detailed measurements, the P-related processes such as ad/desorption and uptake represented in these models are under-constrained and likely oversimplified, thus the future predictions of Amazon forest responses to eCO$_2$ and climate change are uncertain. To fill this gap, in this study, we use data collected as part of the Amazon Fertilization Experiment (AFEX), the first project that focuses on experimental soil nutrient manipulation in the Amazon, with a comprehensive data collection program covering plant ecophysiology, C stocks and fluxes, soil processes including P stocks. Thus, our model parameterization compared to prior P modelling studies includes detailed P processes representation using the site measurements.

Here, we describe the development and implementation of the terrestrial P cycle in the Joint UK Land Environment Simulator (JULES) (Clark *et al.*, 2011), the land component of the UK Earth System Model (UKESM), following the structure of the prior N cycle development (Wiltshire *et al.*, 2021) and utilising state of the art already tested and implemented descriptions of P cycling in other land surface models (Wang, Houlton and Field, 2007; Zhu *et al.*, 2016; Goll *et al.*, 2017).
The model (JULES-CNP) is parameterized and calibrated using novel in situ P soil and plant data from a well-studied forest site in Central Amazon near to Manaus, Brazil with soil P content representative of 60% of soils across the Amazon basin. The new developed P component estimates the sorption of the soil organic and inorganic P based on the saturation status of the adsorbed P pools, which is unique compared to the other existing P models and enable more realistic estimation of P ad/desorption processes. We first evaluate the model at our study site but also at additional five test sites across the Amazon, in Panama and Hawaii. We then apply the model under ambient and eCO$_2$ following the protocol of Fleischer *et al.*, (2019) to predict nutrient limitations on land biogeochemistry under these conditions. Predictions of the CO_2 fertilization effect in JULES-CNP are compared to those in current versions of the model with coupled C and N cycles (JULES-CN) and with C cycle only (JULES-C).

2. Material and methods

2.1 JULES

JULES is a process-based model that integrates water, energy, C cycling (JULES-C) (Clark *et al.*, 2011) and N cycling (JULES-CN) (Wiltshire *et al.*, 2021) between the atmosphere, vegetation and soil (Best *et al.*, 2011; Clark *et al.*, 2011). Vegetation dynamics are represented in JULES using the TRIFFID model, using nine distinct plant functional types (PFTs) (tropical and temperate broadleaf evergreen trees, broadleaf deciduous trees, needle-leaf evergreen and deciduous trees, C3 and C4 grasses, and evergreen and deciduous shrubs), as well as height competition (Harper *et al.*, 2016). Leaf-level photosynthesis (Collatz *et al.*, 1991; Collatz, Ribas-Carbo and Berry, 1992) is scaled to estimate canopy level Gross Primary Productivity (GPP) using a multilayer approach that accounts for vertical variation of radiation interception and partition of sunlit and shaded leaves and associated vertical variation of leaf N and P -exponential decrease through the canopy (Clark *et al.*, 2011:Mercado *et al* 2007, Mercado et al 2009) - while the C:P and N:P ratios remain the same. NPP is estimated as the difference between GPP and autotrophic respiration for each living tissue (leaf, wood, root). NPP is then allocated to increase tissue C stocks and to spread, i.e., expand the fractional coverage of the PFT. The resultant PFT fractional coverages also depend on competition across PFTs for resources, e.g., light. Tissue turnover and vegetation mortality add C into the litter pools. Representation of soil organic C (SOC) follows the Rothamsted Carbon model RothC equations (Jenkinson *et al.*, 1990; Jenkinson and Coleman, 2008) defining four C pools: decomposable plant material (DPM) and resistant plant material (RPM), which receive direct input from litterfall, and microbial biomass (BIO) and humified material (HUM) which receive a fraction of decomposed C from DPM and RPM which is not released to the atmosphere. The limitation of N on SOC is applied to the vegetation and soil components using a dynamic C:N ratio to modify the mineralization and immobilization processes as described in Wiltshire *et al.*, (2021). Note that the soil component of JULES-CN can be run either as a single box model or vertically resolved over soil depth (JULES-CN layered), and in this paper we build upon the vertically resolved version described in Wiltshire et al. (2021).

2.2 JULES-CNP

JULES-CNP includes the representation of the P cycle in JULES version (vn5.5) and it is built on existing and well tested representations of P cycling in other global land surface models (Wang, Houlton and Field, 2007; Yang *et al.*, 2014; Goll *et al.*, 2017; Sun *et al.*, 2021). It includes P fluxes within the vegetation and soil components, and the specification of P pools and processes related to P cycling within the soil column (Fig. 1). A parent material pool is introduced to consider the input of weathered P. The adsorbed, desorbed and occluded fractions of P for both organic and inorganic P are also represented. However, except for parent material and occluded P pools, all other pools are estimated at each soil layer. The description of changes in pools and associated relative fluxes are explained in detail in the next sections. Although JULES-CN includes N leaching and deposition, P leaching and deposition are not included in the current version of JULES-CNP.
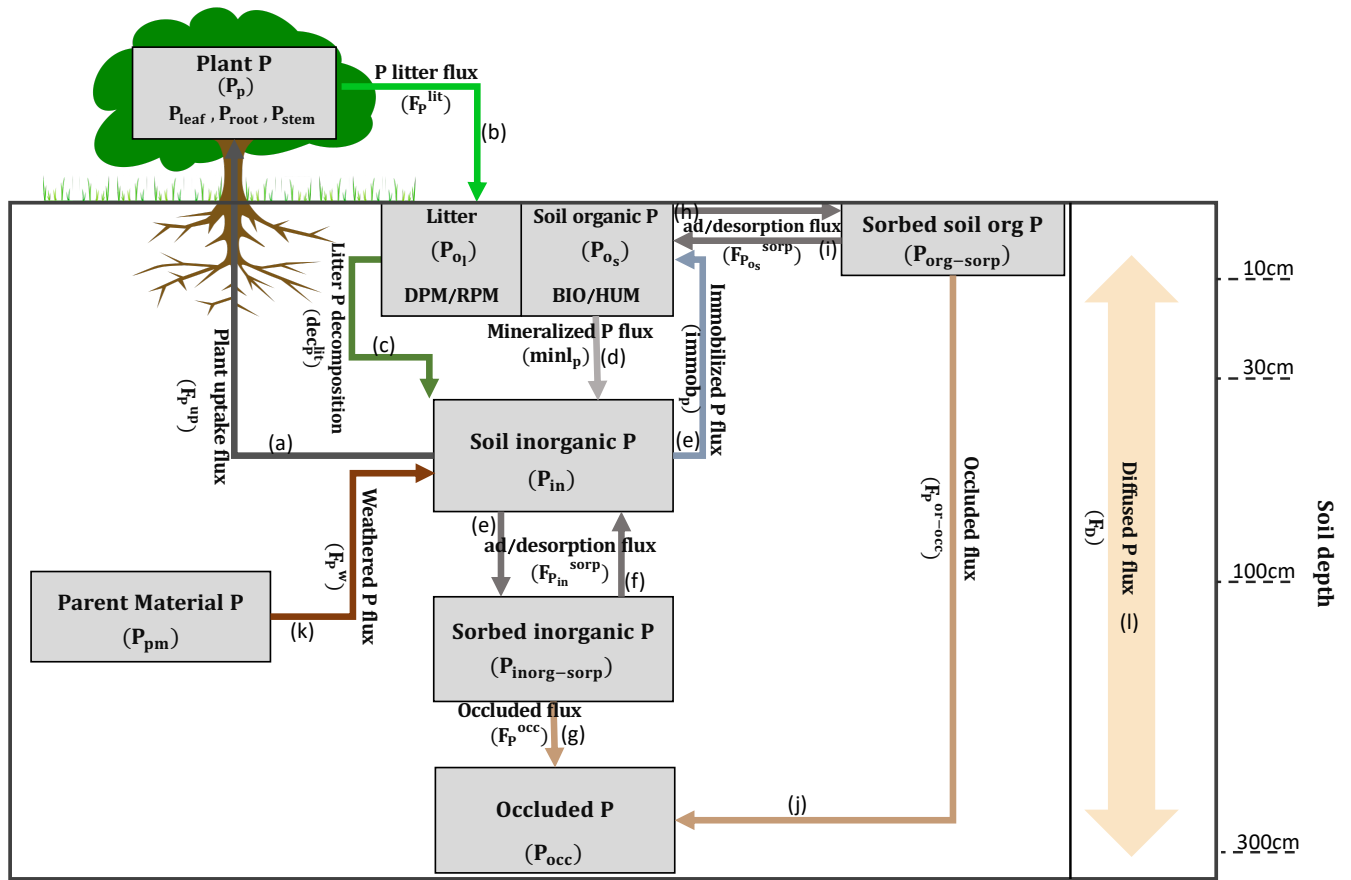
Figure.1 – JULES-CNP model scheme including P pools (grey boxes) and fluxes (arrows)

2.2.1 P pools

JULES represents eight P pools comprising organic and inorganic P: plant P (P_p) and soil P pools (in each soil layer (n)), litter P (P_{O_l}), soil organic P (P_{O_s}), soil inorganic P (P_{in}), organic sorbed ($P_{org-sorp}$), inorganic sorbed ($P_{inorg-sorp}$), parent material (P_{pm}) and occluded (P_{occ}) P comprised of both organic and inorganic P. All pools are in units of kg P m^{-2} (Fig 1, Tables 1 and 2).

Plant P pool is composed of leaf (P_{leaf}), fine root (P_{root}) and stem together with coarse root (P_{stem}), which are related to their associated C pools ($C_{leaf}, C_{root}, C_{stem}$) in (kg C m^{-2}) and fixed C to P ratios ($C{:}P_{leaf}, C{:}P_{root} C{:}P_{stem}$) as follows:

$$P_{leaf} = \frac{C_{leaf}}{C{:}P_{leaf}}$$

(eq.1)

195   $P_{root} = \frac{C_{root}}{C:P_{root}}$ (eq.2)

196

197   $P_{stem} = \frac{C_{stem}}{C:P_{stem}}$ (eq.3)

198

199 Therefore, the plant P pool (P_p) is the sum of all vegetation P pools as follows:

200

201   $P_p = P_{leaf} + P_{root} + P_{stem}$ (eq.4)

202

203 Description of the plant P pool (P_p) follows Zhu *et al.*, (2016) and is estimated as the difference between the

204 input, plant uptake $F_P{}^{Up}$ (eq.26) and output of this pool, plant litter flux $F_P{}^{lit}$ (eq.28), with both fluxes

205 expressed in kg P m^{-2} yr^{-1} as follows:

206

207   $\frac{dP_p}{dt} = F_P{}^{up} - F_P{}^{lit}$ (eq.5)

208

209 The litter P pool (P_{O_l}) is estimated as a sum of P_{DPM} and P_{RPM} pools over soil layers (n). Each pool is formed by

210 the fluxes of plant litter input ($F_P{}^{lit}$) and the outgoing decomposed P ($dec_P{}^{lit}$) both expressed in kg P m^{-2} yr^{-1}

211 (eq.28-29). Furthermore, the plant litter input is modified based on the plant type material ratio α (in order to

212 distribute the litter input based on the DPM/RPM fraction) as follows:

213

214   $\frac{dP_{DPM}}{dt} = F_{P_n}{}^{lit} \times \alpha - dec_{P_{DPM,n}}$ (eq.6)

215

216   $\frac{dP_{RPM}}{dt} = F_{P_n}{}^{lit} \times (1 - \alpha) - dec_{P_{RPM,n}}$ (eq.7)

217

218   $P_{O_l} = \sum_{n=1}^{N} P_{DPM_n} + \sum_{n=1}^{N} P_{RPM_n}$ (eq.8)

219

220 The soil organic pool (P_{O_s}) is represented as the sum of P_{BIO} and P_{HUM}. These pools are estimated from the

221 difference between P inputs from total immobilized (F_{immob_P}) distributed between BIO and HUM based on

222 fixed fraction (0.46 for BIO, 0.54 for HUM) (Jenkinson *et al.*, 1990; Jenkinson and Coleman, 2008) and

223 desorbed P, $F_{P_{O_s}}{}^{desorp}$ and P outputs from mineralized (F_{minl_P}), and adsorbed P fluxes ($F_{P_{O_s}}{}^{sorp}$) (adsorption:

224 eq. 40 and desorption: eq.41) with all fluxes expressed in kg P m^{-2} yr^{-1} as follows:

225

226   $\frac{dP_{BIO}}{dt} = 0.46 \times F_{immob_{P_n}} + F_{P_{O_{S_{BIO,n}}}}{}^{desorp} - F_{minl_{P_{BIO,n}}} - F_{P_{O_{S_{BIO,n}}}}{}^{sorp}$ (eq.9)

227

228   $\frac{dP_{HUM}}{dt} = 0.54 \times F_{immob_{P_n}} + F_{P_{O_{S_{HUM,n}}}}{}^{desorp} - F_{minl_{P_{BIO,n}}} - F_{P_{O_{S_{HUM,n}}}}{}^{sorp}$ (eq.10)

229

230   $P_{O_s} = \sum_{n=1}^{N} P_{BIO_n} + \sum_{n=1}^{N} P_{HUM_n}$ (eq.11)

231

232

233 Description of the inorganic sorbed P pool ($P_{inorg-sorp}$) follows Wang *et al.*, (2007) and is represented as the

234 difference between the input flux of inorganic sorption ($F_{P_{in}}{}^{sorp}$) (eq. 37) and output fluxes of inorganic

235 desorption ($F_{P_{in}}{}^{desorp}$) (eq. 38) and occluded P ($F_P{}^{occ}$) (eq. 39), with all fluxes expressed in kg P m^{-2} yr^{-1} as

236 follows:

237

238   $\frac{dP_{inorg-sorp}}{dt} = \sum_{n=1}^{N} F_{P_{in_n}}{}^{sorp} - \sum_{n=1}^{N} F_{P_{in_n}}{}^{desorp} - \sum_{n=1}^{N} F_{P_n}{}^{occ}$ (eq.12)

239

240 The description of the occluded (P_{occ}) P pool follows Wang *et al.*, (2007) and Hou *et al.*, (2019) and is

241 represented as the sum of input fluxes of occluded P from both organic ($F_P{}^{or-occ}$) (eq. 42) and inorganic P

242 pools ($F_P{}^{occ}$) expressed in kg P m^{-2} yr^{-1}, as follows:

243

244   $\frac{dP_{occ}}{dt} = \sum_{n=1}^{N} F_{P_n}{}^{occ} + \sum_{n=1}^{N} F_{P_n}{}^{or-occ}$ (eq.13)

245

246 The description of the organic sorbed P pool ($P_{org-sorp}$) follows Wang *et al.*, (2007) and is represented as the
247 difference between the input flux of organic sorption ($F_{P_{OS_n}}{}^{sorp}$) and output fluxes of organic desorption
248 ($F_{P_{OS_n}}{}^{desorp}$) and occluded P($F_{P_n}{}^{occ}$), with all fluxes expressed in kg P m^{-2} yr^{-1} as follows:

$$\frac{dP_{org-sorp}}{dt} = \sum_{n=1}^{N} F_{P_{OS_n}}{}^{sorp} - \sum_{n=1}^{N} F_{P_{OS_n}}{}^{desorp} - \sum_{n=1}^{N} F_{P_n}{}^{or-occ} \qquad (eq.14)$$

254 P from parent material (P_{pm}) pool follows Wang *et al.*, (2007) and depends on the weathering flux ($F_P{}^w$) (eq.
255 43) in kg P m^{-2} yr^{-1} as follows:

$$\frac{dP_{pm}}{dt} = -\sum_{n=1}^{N} F_{P_n}{}^{w} \qquad (eq.15)$$

2.2.2. C and P fluxes

262 NPP in JULES is calculated as the difference between GPP and autotrophic respiration. In JULES-CNP,
263 potential NPP represents the amount of C, available for tissue growth (C density increase) on a unit area, and
264 spreading (vegetation cover increase as a result of reproduction and recruitment), i.e., to increase the area
265 covered by the vegetation type, assuming no nutrient limitation. The reported NPP in the literature often
266 includes other C fluxes related to the exudates, production of volatiles and non-structural carbohydrates (Malhi
267 *et al.*, 2009; Chapin *et al.*, 2011; Walker *et al.*, 2021) which are challenging to measure (Malhi, Doughty and
268 Galbraith, 2011). Therefore, actual NPP is for our purposes equal to Biomass Production (BP), and is calculated
269 as potential NPP minus excess C (lost to the plant through autotrophic respiration), with the latter the C that
270 cannot be used to grow new plant tissue due to insufficient plant nutrient supply. Hence, if the system is limited
271 by the availability of N and/or P, NPP will be adjusted to match the growth that can be supported with the
272 limited N or P supply, with any excess carbohydrate lost through excess C.
273 The total excess C term (ψ_t) (kg C m^{-2} yr^{-1}) is calculated as:

$$\psi_t = \psi_g + \psi_s \qquad (eq.16)$$

277 where ψ_g and ψ_s are the excess C fluxes due to growth (g) and spread (s) and are assumed to be rapidly respired
278 by plants.

280 Therefore, BP is calculated as the difference between potential NPP (Π_c) and total excess C:

$$BP = \Pi_c - \psi_t \qquad (eq.17)$$

284 The litter production in JULES before limitation is estimated as follows:

$$F_{C_n}^{lit} = \gamma_{leaf} C_{leaf} + \gamma_{root} C_{root} + \gamma_{wood} C_{wood} \qquad (eq.18)$$

288 where γ is a temperature dependent turnover rate representing the phenological state (Clark *et al.*, 2011). P
289 limitation is applied on the C litter production similar to the N scheme of JULES (JULES-CN) (Wiltshire *et al.*,
290 2021). In JULES-CN the N limitation effect on the litter production is captured by estimating the available C for
291 litter production as a difference between the NPP and excess C (Wiltshire *et al.*, 2021).

293 Similar to other P-enabled models (Yang *et al.*, 2014; Goll *et al.*, 2017), JULES-CNP follows the same structure
294 as its N model component. Description of the plant P and N demand follow Wang *et al.*, (2007) and are
295 represented by the sum of demand ($\emptyset_t$) to sustain growth (P-related: ($\emptyset_{g_P}$), N-related: ($\emptyset_{g_N}$)) and to sustain
296 vegetation spreading (to increment PFT fractional coverage) (P-related: ($\emptyset_{S_P}$), N-related: ($\emptyset_{S_N}$)) and is
297 expressed in (P-related in kg P m^{-2} yr^{-1}; N-related in kg N m^{-2} yr^{-1}). The total demand for growth ($\emptyset_g$) and
298 spreading ($\emptyset_s$) is controlled by the dominant demand between P ($\emptyset_{g_P}$) and N ($\emptyset_{g_N}$) as follows:

$$\emptyset_t = \emptyset_g + \emptyset_s \qquad (eq.19)$$

301 $\emptyset_{gP} = \frac{P_p}{C_V}\left(\Pi_c - \frac{dC_v}{dt} - \psi_g\right)$ (eq.20)

302 $\emptyset_{sP} = \frac{P_p}{C_V}\left(\Pi_c - \frac{dC_v}{dt} - \psi_s\right)$ (eq.21)

303 $\emptyset_{gN} = \frac{N_v}{C_V}\left(\Pi_c - \frac{dC_v}{dt} - \psi_g\right)$ (eq.22)

304 $\emptyset_{sN} = \frac{N_v}{C_V}\left(\Pi_c - \frac{dC_v}{dt} - \psi_s\right)$ (eq.23)

305 $\emptyset_g = \begin{cases} \emptyset_{gP} & \emptyset_{gP} \times \frac{C_V}{P_p} > \emptyset_{gN} \times \frac{C_V}{N_v} \\ \emptyset_{gN} & \emptyset_{gN} \times \frac{C_V}{N_v} > \emptyset_{gP} \times \frac{C_V}{P_p} \end{cases}$ (eq.24)

306 $\emptyset_s = \begin{cases} \emptyset_{sP} & \emptyset_{sP} \times \frac{C_V}{P_p} > \emptyset_{sN} \times \frac{C_V}{N_v} \\ \emptyset_{sN} & \emptyset_{sN} \times \frac{C_V}{N_v} > \emptyset_{sP} \times \frac{C_V}{P_p} \end{cases}$ (eq.25)

307
308
309 where $\frac{P_p}{C_V}$ is the inverse of whole plant C:P ratio, $\frac{N_v}{C_V}$ is inverse plant C:N ratio, $\frac{dC_v}{dt}$ is rate of change in plant C
310 (see Clark *et al.,* (2011) for more detail), Π_c is nutrient-unlimited, or potential, NPP (kg C m^{-2} yr^{-1}), ψ_g is excess
311 C due to either P or N limitation for plant growth (kg C m^{-2} yr^{-1}) and ψ_s is excess C due to either P or N
312 limitation for vegetation spreading (kg C m^{-2} yr^{-1}).
313
314 Equations 20 and 22 are solved by first setting $\psi_g = 0.0$ to find the total plant P (eq. 20) and N demand (eq.22).
315 If the P and N demand for growth are less than the available P and N and fractional coverage (λ) (NPP fraction
316 used for fractional cover increment; for detail see Wiltshire *et al.,* (2021)) at the considered timestep Δt then
317 there is no limitation to growth ($i.e. \emptyset_{gP} < \frac{(1-\lambda)P_{avail}}{\Delta t}$; $\emptyset_{gN} < \frac{(1-\lambda)N_{avail}}{\Delta t}$). Where there is limited P and/or N
318 availability, the uptake equals the available P and N ($\emptyset_{gP} = \frac{(1-\lambda)P_{avail}}{\Delta t}$; $\emptyset_{gN} = \frac{(1-\lambda)N_{avail}}{\Delta t}$), and the plant
319 growth which cannot be achieved due to nutrient constraints will be deducted from potential NPP, here termed
320 excess C term (ψ_g), to give an actual NPP. Following Wiltshire et al., 2021, we assume excess C is respired by
321 the plant.
322
323 Similarly, in order to estimate the P and N demand for spreading (eq. 21 and 23), initially the excess C from
324 spreading is set to 0.0 ($\psi_s = 0.0$), i.e under the assumption that there is no nutrient limitation. If the P and N
325 demand for spreading are lower than the available P and N and fractional coverage (λ) ($\emptyset_{sP} <$
326 $\frac{(1-\lambda)P_{avail}}{\Delta t}$; $\emptyset_{sN} < \frac{(1-\lambda)N_{avail}}{\Delta t}$), then there is no limitation on spreading and in case of limited P and N
327 availability, the uptake equals the available P and N ($\emptyset_{sP} = \frac{(1-\lambda)P_{avail}}{\Delta t}$; $\emptyset_{sN} = \frac{(1-\lambda)N_{avail}}{\Delta t}$), and the excess C
328 for spread (ψ_s) is subtracted from potential NPP.
329
330 Plant P uptake ($F_p{}^{up}$) (arrow a in Fig 1) is estimated based on the P demand for growth and spreading ($\emptyset_t$) and
331 the root uptake capacity (u^{max}) (kg P kg^{-1} C yr^{-1}), as follows:
332
333 $F_p{}^{up}{}_n = \begin{cases} \emptyset_t & \emptyset_t \leq u^{max} \\ u^{max} & \emptyset_t > u^{max} \end{cases}$ (eq.26)

334
335 Plant P uptake ($F_p{}^{up}$) varies spatially depending on the root uptake capacity (u^{max}) followed by Goll *et al.,*
336 (2017). Therefore, in regions with limited P supply, the plant P uptake is limited to the u^{max} and consequently
337 impacts the excess C and BP.
338 The root uptake capacity depends on the maximum root uptake capacity (v_{max}) (kg P kg^{-1} C yr^{-1}), root depth
339 (d_{root}), the concentration of inorganic P at different soil depths (P_{in}), and a half saturation term at which half of
340 the maximum uptake capacity is reached using inorganic P at different soil depths (P_{in}), a scaling uptake ratio
341 (K_p) (μmol P l^{-1}), unit conversion (C_f) (1 kg P^{-1}), and soil moisture (θ) (l m^{-2}), as follows:
342
343 $u^{max} = v_{max} \times d_{root} \times \sum_{n=1}^{N} P_{in_n} \times \left(\frac{1}{\sum_{n=1}^{N} P_{in_n} + c_f \times K_p \times \theta_n}\right)$ (eq.27)

344

Description of the litter production of P ($F_{P_n}^{lit}$) (arrow b in Fig 1) follows JULES-CN as in Wiltshire *et al.*, (2021) and is calculated based on the litter flux of C (kg C m^{-2} yr^{-1}) using leaf, root and wood turnovers (yr^{-1}), and through the vegetation dynamics due to large-scale disturbance and litter production density, as follows:

$$F_{P_n}^{lit} = \left(\frac{(1-k_{leaf})\gamma_{leaf}C_{leaf}}{C:P_{leaf}}\right) + \left(\frac{(1-k_{root})\gamma_{root}C_{root}}{C:P_{root}}\right) + \left(\frac{\gamma_{wood}C_{wood}}{C:P_{stem}}\right) \qquad (eq.28)$$

where λ is the leaf, root and stem re-translocation (at daily timestep) coefficient (Zaehle and Friend, 2010; Clark *et al.*, 2011) and the related $C:P$ ratios for P fraction and γ is a temperature dependent turnover rate representing the phenological state (Clark *et al.*, 2011).

The decomposition of litter (dec^{lit}) (arrow c in Fig 1) depends on soil respiration (R) (kg C m^{-2} yr^{-1}), the litter C:P ratio ($C:P_{lit}$) at each soil layer (n) as follows:

$$dec_P{}^{lit} = \frac{\sum_{n=1}^{N} R_n}{C:P_{lit}} \qquad (eq.29)$$

where the $C:P_{lit}$ is calculated based on litter C pool (DPM and RPM) (lit^C) (kg C m^{-2} yr^{-1}) and litter P pool (P_{O_l}) as follows:

$$C:P_{lit} = \frac{\sum_{n=1}^{N} lit_n{}^C}{P_{O_{l_n}}} \qquad (eq.30)$$

The mineralized (F_{minl_P}) (arrow d in Fig 1) and immobilized (F_{immob_P}) (arrow e in Fig 1) P fluxes are calculated based on C mineralization and immobilization, C:P ratios of plant (i) (DPM/RPM) ($C:P_{plant}$) and soil (HUM/BIO) ($C:P_{soil}$), soil pool potential respiration (R_{POT_i}) (kg C m^{-2} yr^{-1}) and the respiration partitioning fraction (*resp_frac*) as follows:

$$F_{minl_{P_n}} = \frac{\sum_{n=1}^{N} R_{POT_{i,n}}}{C:P_{plant}} \qquad (eq.31)$$

$$F_{immob_{P_n}} = \frac{\sum_{n=1}^{N} R_{i,n} \times resp\_frac}{C:P_{soil}} \qquad (eq.32)$$

The soil respiration from each soil layer ($R_{i,n}$) is estimated from potential soil respiration ($R_{POT_{i,n}}$) for the DPM, RPM pools and the litter decomposition rate modifier (F_{P_n}) as follows:

$$R_{i,n} = R_{POT_{i,n}} \times F_{P_n} \qquad (eq.33)$$

where the description of F_{P_n} for P pools ($F_{P_{P_n}}$) follows Wang *et al.*,(2007) and is estimated based on the soil pool (BIO/HUM) mineralization ($minl_{P-BIO_n}$, $minl_{P-HUM_n}$) and immobilization ($immob_{P-BIO_n}$, $immob_{P-HUM_n}$) (in kg P m^{-2} yr^{-1}), soil inorganic P (P_{inorg_n}) (in kg P m^{-2}), and litter pools (DPM/RPM) demand (in kg P m^{-2} yr^{-1}) as follows:

$$F_{P_{P_n}} = \frac{(minl_{P-BIO_n} + minl_{P-HUM_n} - immob_{P-BIO_n} - immob_{P-HUM_n}) + P_{inorg_n}}{DEM_{DPM_n} + DEM_{RPM_n}} \qquad (eq.34)$$

The net demand associated with decomposition of litter pools ($DEM_{k,n}$) represents the P required by microbes which convert DPM and RPM into BIO and HUM. The limitation due to insufficient P availability is estimated based on the potential mineralization ($minl_{p-pot}$) and immobilization ($immob_{p-pot}$) (in kg P m^{-2} yr^{-1}) of pools (k) as follows:

$$DEM_{k,n} = immob_{p-pot,k} - minl_{p-pot,k} \qquad (eq.35)$$

The F_{P_n} estimated for N pools ($F_{P_{N_n}}$) follows the same formulation as P (see Wiltshire *et al.*, 2021 for further details) and the F_{P_n} is estimated based on a higher rate modifier between N and P as follows:

397 $$F_{P_n} = \begin{cases} F_{P_{P_n}} & F_{P_{P_n}} > F_{P_{N_n}} \\ F_{P_{N_n}} & F_{P_{N_n}} > F_{P_{P_n}} \end{cases}$$ (eq.36)

398

399 Description of the fluxes of adsorption ($F_{P_{in_n}}{}^{sorp}$) (arrow e in Fig 1) and desorption ($F_{P_{in_n}}{}^{desorp}$) (arrow f in Fig

400 1) of inorganic P in kg P m^{-2} yr^1 follow Wang *et al.*, (2010) and are calculated based on soil inorganic (P_{in_n}) and

401 sorbed inorganic ($P_{inorg-sorbed_n}$) P pools and inorganic adsorption ($K_{sorp-in}$), desorption ($K_{desorp-in}$)

402 coefficients (kg P m^{-2} yr^{-1}) and maximum sorbed inorganic (P_{in-max}) (kg P m^{-2}) as follows:

403

404 $$F_{P_{in_n}}{}^{sorp} = P_{in_n} \times K_{sorp-in} \times \frac{\left(P_{in-max_n} - P_{inorg-sorbed_n}\right)}{P_{in-max_n}}$$ (eq.37)

405

406 $$F_{P_{in_n}}{}^{desorp} = P_{inorg-sorbed_n} \times K_{desorp-in}$$ (eq.38)

407

408 Description of the occluded inorganic P flux ($F_{P_n}{}^{occ}$) (arrow g in Fig 1) follows Wang *et al.*, (2007) and Hou *et*

409 *al.*, (2019) and is calculated based on sorbed inorganic P pool and P occlusion rate (K_{occ}) (kg P m^{-2} yr^{-1}) as

410 follows:

411

412 $$F_{P_n}{}^{occ} = P_{inorg-sorbed_n} \times K_{occ}$$ (eq.39)

413

414 Description of the fluxes of adsorption ($F_{P_{O_{S_n}}}{}^{sorp}$) (arrow h in Fig 1) and desorption ($F_{P_{O_{S_n}}}{}^{desorp}$) (arrow i in Fig

415 1) of organic P follow Wang *et al.*, (2010) are calculated based on soil organic and sorbed organic P pools and

416 organic adsorption ($K_{sorp-or}$) (kg P m^{-2} yr^{-1}), desorption ($K_{desorp-or}$) coefficients (kg P m^{-2} yr^{-1}) and maximum

417 sorbed organic ($P_{org-max}$) (which corresponds to the sorbed soil P saturation, thus modifying the sorption rate

418 respectively) (kg P m^{-2}) as follows:

419

420 $$F_{P_{O_{S_n}}}{}^{sorp} = P_{O_{S_n}} \times K_{sorp-or} \times \frac{\left(P_{or-max_n} - P_{org-sorbed_n}\right)}{P_{or-max_n}}$$ (eq.40)

421

422 $$F_{P_{O_{S_n}}}{}^{desorp} = P_{org-sorbed_n} \times K_{desorp-or}$$ (eq.41)

423

424 Description of the occluded organic P flux ($F_{P_n}{}^{or-occ}$) (kg P m^{-2} yr^{-1}) (arrow j in Fig 1) follows Wang *et al.*,

425 (2007) and Hou *et al.*, (2019) is calculated based on sorbed organic P pool ($P_{org-sorbed_n}$) and P occlude rate

426 (K_{occ}) (kg P m^{-2} yr^{-1}) as follows:

427

428 $$F_{P_n}{}^{or-occ} = P_{org-sorbed_n} \times K_{occ}$$ (eq.42)

429

430 Description of the P flux from weathered parent material ($F_{P_n}{}^{w}$) (arrow k in Fig 1) follows Wang *et al.*, (2007)

431 and is calculated based on amount of P in the parent material (P_{pm}) and P weathering rate (K_w) (kg P m^{-2} yr^{-1}) as

432 follows:

433

434 $$F_{P_n}{}^{w} = P_{pm_n} \times K_w$$ (eq.43)

435

436 Description of P diffusion between soil layers (F_{D_n}) expressed in (kg P m^{-2} yr^{-1}) (arrow l in Fig 1) follows Goll

437 *et al.*, (2017) and is calculated following Fick's second law and it is a function of the diffusion coefficient (Dz)

438 in m^2 s^{-1}, the concentration of inorganic P at different soil depths (P_{in}) in kg P m^{-2}, the distance (z) between the

439 midpoints of soil layers in metres and seconds to year unit conversion (Yr):

440

441 $$F_{D_n} = \frac{\partial}{\partial z}\left(D_{z_n} \frac{\partial P_{s_n}}{\partial z}\right) \times Yr$$ (eq.44)

442

443

444

445

446

Table 1. Model variables

Variable	Unit	Definition
ψ	kg C m^{-2} yr^{-1}	Excess C flux
$\emptyset$	kg P m^{-2} yr^{-1}	Plant demand for uptake
Π_c	kg C m^{-2} yr^{-1}	Potential NPP
u^{max}	kg P kg^{-1} C yr^{-1}	Root uptake capacity
DEM	kg P m^{-2} yr^{-1}	Plant pool P associated decomposition demand
$dec_P{}^{lit}$	kg P m^{-2} yr^{-1}	Litter decomposition
F_D	kg P m^{-2} yr^{-1}	Plant diffusion flux
F_P	-	Plant litter decomposition rate modifier
$F_p{}^{lit}$	kg P m^{-2} yr^{-1}	Plant litter flux
$F_p{}^{up}$	kg P m^{-2} yr^{-1}	Plant uptake
$F_{P_{O_S}}{}^{sorp}$	kg P m^{-2} yr^{-1}	Sorbed organic P flux
$F_{P_{in}}{}^{sorp}$	kg P m^{-2} yr^{-1}	Sorbed inorganic P flux
$F_{P_{O_S}}{}^{desorp}$	kg P m^{-2} yr^{-1}	Desorbed organic P flux
$F_{P_{in}}{}^{desorp}$	kg P m^{-2} yr^{-1}	Desorbed inorganic P flux
$F_p{}^{occ}$	kg P m^{-2} yr^{-1}	Occluded inorganic P flux
$F_p{}^{or-occ}$	kg P m^{-2} yr^{-1}	Occluded organic P flux
$F_p{}^{w}$	kg P m^{-2} yr^{-1}	Weathered P flux
$F_{immob\,P}$	kg P m^{-2} yr^{-1}	Immobilized P flux
lit_C	kg C m^{-2} yr^{-1}	C litter flux
lit_{frac}	-	Litter fraction
lit_{leaf}	kg C m^{-2} yr^{-1}	Leaf litter flux
lit_{root}	kg C m^{-2} yr^{-1}	Root litter flux
lit_{wood}	kg C m^{-2} yr^{-1}	Woody litter flux
$F_{minl\,P}$	kg P m^{-2} yr^{-1}	Mineralized P flux
P_p	kg P m^{-2}	Plant P pool
P_{O_l}	kg P m^{-2}	Litter organic pool
P_{O_s}	kg P m^{-2}	Soil organic pool
P_{in}	kg P m^{-2}	Soil inorganic pool
$P_{inorg-sorp}$	kg P m^{-2}	Soil inorganic sorbed pool
$P_{org-sorp}$	kg P m^{-2}	Soil organic sorbed pool
P_{occ}	kg P m^{-2}	Soil occluded pool
P_{pm}	kg P m^{-2}	Parent material pool
R	kg C m^{-2} yr^{-1}	Total respiration
R_{POT}	kg C m^{-2} yr^{-1}	Total potential respiration
R^s	kg C m^{-2} yr^{-1}	Soil respiration
R_d	kg C m^{-2} yr^{-1}	Leaf dark respiration
T_{ref}	K	Soil reference temperature
T_s	K	Soil temperature
Veg$_c$	kg C m^{-2}	Sum of biomass
z	m	Soil depth

455

Table 2. P Model parameters

Parameter	Value	Unit	Eq.	Description	Source
C and N related					
α	0.25	-	6	Plant type material ratio	(Clark *et al.*, 2011)
a_{wl}	1.204	kg C m^{-2}	50	Allometric coefficient	calibrated
σ_l	0.0375	kg C m^{-2} per unit LAI	48	Specific leaf density	Clark *et al.*, 2011
b_{wl}	1.667	-	50	Allometric exponent.	Clark *et al.*, 2011
f_{dr}	0.005	-	47	Respiration scale factor	Calibrated
$resp\_frac$	0.25	-	32	Respiration fraction	(Clark *et al.*, 2011)
k_{leaf}	0.5	-	28	Leaf N re-translocation coefficient	(Zaehle and Friend, 2010)
k_{root}	0.2	-	28	Root N re-translocation coefficient	(Zaehle and Friend, 2010)
d_{root}	3.0	-	27	Root fraction in each soil layer	(Clark *et al.*, 2011)
v_{int}	7.21	µmol CO$_2$ m^{-2} s^{-1}	45	Intercept in the linear regression between V_{cmax} and N_{area}	Calibrated (Clark *et al.*, 2011)
v_{sl}	19.22	µmol CO$_2$ gN^{-1} s-1	45	Slope in the linear regression between V_{cmax} and N_{area}	Calibrated (Clark *et al.*, 2011)
LMA	131.571852	g m-2	45	Observed Leaf Mass per Area	Study site
Leaf N	1.79007596	g g-1	45, 46	Foliar N concentrations	Study site
P related					
$C{:}P_{soil}$	1299.6	-	32	Soil C:P ratio	(Fleischer *et al.*, 2019)
v_{max}	0.0007	kg P kg^{-1} C yr^{-1}	27	Maximum root uptake capacity	Calibrated (Goll *et al.*, 2017)
P	0.7083062	g kg^{-1}	46	Foliar P concentrations	Study site
c_f	3.1×10^{-5}	1 kg P^{-1}	27	Conversion factor	(Goll *et al.*, 2017)
D_z	0.001	m^2 s^{-1}	44	Diffusion coefficient	(Burke *et al*, 2017)
K_{occ}	1.2×10^{-5}	yr^{-1}	39, 42	P occlusion rate	(Yang *et al.*, 2014)
K_p	3.0	kg P l^{-1}	27	Scaling uptake ratio	Calibrated
$K_{sorp-in}$	0.0054	kg P m^{-2} yr^{-1}	37	Inorganic P adsorption coefficient	Calibrated (Hou *et al.*, 2019)
$K_{sorp-or}$	0.00054	kg P m^{-2} yr^{-1}	40	Organic P adsorption coefficient	Calibrated
K_{in-max}	0.0075	kg P m^{-2} yr^{-1}	37	Maximum sorbed inorganic P	Study site
K_{or-max}	0.0042	kg P m^{-2} yr^{-1}	40	Maximum sorbed organic P	Study site
K_w	3×10^{-6}	kg P m^{-2} yr^{-1}	43	P weathering rate	(Wang *et al.*, 2010)

456
457 **2.3 Study sites**
458

This study primarily uses data from two nearby sites in Central Amazon in Manaus, Brazil. The main site from here on termed *study site* (2°35′′21.08′′ S, 60°06′′53.63′′ W) (Lugli *et al.*, 2020) is for model development and evaluation. The second site is the Manaus K34 flux site (2°36′′32.67′′ S, 60°12′′33.48′′ W) which provides meteorological station data for running the model but also provides data for model evaluation. Our *study site* is the main lowland tropical forest site maintained by the National Institute for Amazon Research (INPA). Research at this site focuses on projects, combining experimental approaches (Keller *et al.*, 2004; Malhi *et al.*, 2009) with modelling (Lapola and Norby, 2014). We use detailed novel soil and plant P pool data from the *study site* (Lugli *et al.*, 2020, 2021) for model parameterisation and calibration and carbon stock data for model validation. The *study site* has a very similar forest, geomorphology, soil chemistry and species composition to the well-known and studied K34 flux site (Araújo *et al.*, 2002). The average reported annual precipitation is 2431 (mm yr^{-1}), with a monthly range of 95 to 304 (mm month^{-1}), and averaged temperature is 26°C (Araújo *et al.*, 2002). Soil type at this site is Geric Ferrosol with a high clay content and weathering activities (Malhi *et al.*, 2004).

472

473 In addition to the *study site* we use data from other P limited locations from the Amazon, Panama and Hawaii
474 (Table 3) for model evaluation. Old-growth forest sites in the Amazon are located across a fertility gradient
475 from west to east (AGP-01, SA3, CAX,) with detailed C cycle measurements available (Aragão *et al.*, (2009)).
476 The site in Panama is located in the Gigante Peninsula in the Barro Colorado Nature Reserve and is a 200 year
477 old semi-deciduous rainforest (Wright *et al.*, 2011) growing on Oxisols developed on Miocene basalt (Dieter,
478 Elsenbeer and Turner, 2010) with the topsoil a dominant clay texture (Turner and Condron, 2013). It is the
479 location of a long term running nutrient fertilization experiment since 1998 (Mirabello *et al.*, 2013). The site in
480 Hawaii (Hawaii Kokee) is a P limited chronosequence that developed on the 4 million year old oxisols soil
481 (Vitousek, 2004) and has a long term fertilization experiment. Site information is provided in Table 3.
482
483 **Table 3.** Test sites name, location and climate characterises.

Site	Name	Location		Climate	
		Lat.	Lon.	Rainfall (mm yr^{-1})	Temperature(°C)
Study site	AFEX project	-2.58	-60.11	2431	26
AGP-01	Agua pudre plot E	-3.72	-70.3	2723	25.5
CAX	Caxiuanã flux tower site	-1.72	-51.5	2314	26.9
SA3	Tapajós flux tower site	-2.5	-55	1968	26.1
Gig. Pen.	Gigante peninsula (control data)	-9.1	-79.84	2600	26
Hawaii K.	Hawaii Kokee (control data)	22.13	-159.62	2500	16

484
485
486 **2.4 Model parameterisation, calibration and evaluation at study site**
487
488 We use observations from the four control plots of the study site to parameterise, calibrate and evaluate different
489 processes in JULES (Table 4). The observations were collected at 4 soil depths and processed using the Hedley
490 sequential fractionation (Hedley, Stewart and Chauhan, 1982; Quesada *et al.*, 2010). Observed Leaf Mass per
491 Area (LMA), leaf N and leaf P estimated from fresh leaves were used as input parameters to JULES to estimate
492 photosynthetic capacity and respiration parameters. JULES vn5.5 (JULES CN in this study) estimates V_{cmax}
493 (µmol m^{-2} s^{-2}) based on Kattge et al. (2009) using foliar N concentrations in area basis ($nleaf$), as follows:
494
495 $$V_{cmax} = v_{int} + v_{sl} * nleaf$$ (eq.45)
496
497 where v_{int} is the estimated intercept and v_{sl} is the slope of the linear regression derived for the V_{cmax} estimation.
498 We incorporated an additional P dependency on the estimation of V_{cmax} following Walker et al. (2014) as
499 follows:
500
501 $$\ln(V_{cmax}) = 3.946 + 0.921\ln(N) + 0.121\ln(P) + 0.282\ln(N)\ln(P)$$ (eq.46)
502
503 Where N and P are foliar concentrations in area basis.
504
505 Implementation of eq. 46 resulted in higher V_{cmax} than in the original version of JULES. A higher V_{cmax} predicted
506 higher leaf and plant respiration (eq.47). Constrained by observations of NPP and plant respiration at the study
507 site, we modified one of the most uncertain parameters in the description of plant respiration (f_{dr}) (eq.47) which
508 is the scale factor for leaf dark respiration (R_d) as follows:
509
510 $$R_d = f_{dr} V_{cmax}$$ (eq.47)
511
512 The default value is 0.01 (Clark *et al.*, 2011), and for JULES-CNP simulations at our study site it was modified
513 to 0.005.
514 Observations of aboveground biomass were used to calibrate the non PFT dependent allometric relationships in
515 JULES (Clark et al 2011) (eq 48-50) for leaf, root and wood C. Specifically, the a_{wl} parameter (eq 50) was
516 modified from 0.65 to 1.204 to match better tropical forest allometry:
517
518 $$C_{leaf} = \sigma_l L_b$$ (eq.48)
519 $$C_{root} = C_{leaf}$$ (eq.49)

520 $C_{stem} = a_{wl} L_b{}^{b_{wl}}$ (eq.50)
521
522 Where σ_l is specific leaf density (kg C m^{-2} per unit LAI), L_b is balanced (or seasonal maximum) leaf area index
523 (m^2 m^{-2}), a_{wl} is allometric coefficient (kg C m^{-2}) and b_{wl} is the allometric exponent.
524 Note that JULES-CNP uses the C3 and C4 photosynthesis model from Collatz et al., 1991; Collatz, Ribas-Carbo
525 and Berry, 1992, which does not include estimation of J$_{max}$.
526
527 JULES-CNP has fixed stoichiometry and C:P ratios of leaf and root (measured), and wood (estimated from fresh
528 coarse wood (Lugli, 2013)) which were taken from the *study site* and prescribed in JULES to simulate P
529 dynamics in the plant. The following belowground data were used to represent various soil P pools: Resin and
530 bicarbonate inorganic P (inorganic P: P_{in}), organic bicarbonate P (organic P: P_{O_S}), NaOH organic P (sorbed
531 organic P: $P_{org-sorp}$), NaOH inorganic P (sorbed inorganic P: $P_{inorg-sorp}$), residual P (occluded P: P_{occ}) and
532 HCL P (parent material P: P_{pm}) (Table 4). The measurements were collected between 2017 and 2018 in control
533 plots. All measurements were conducted in four soil layers (0-5 ,5-10, 10-20, 20-30 cm). However, to be
534 consistent with the JULES model soil layer discretization scheme, we defined 4 soil layers (0-10 cm, 10-30 cm,
535 30-100 cm and 100-300 cm) and we used the average between 0 and 30 cm to compare against the measurement
536 from the same depth for model evaluation.
537 Vegetation C stocks were derived based on tree diameter measurements at breast height, that are linked to
538 allometric equations and wood density databases to estimate the C stored in each individual tree, and then scaled
539 to the plot (Chave *et al.*, 2014).
540
541 The organic and inorganic soil P was assumed to be always at equilibrium with the relative sorbed pools (Wang,
542 Law and Pak, 2010). Thus, in order to cap P sorption and uptake capacity, the maximum sorption capacities
543 (P_{in-max_n}, P_{or-max_n}, eq.37 and 39) (adopted from (Wang, Houlton and Field, 2007)) were prescribed using
544 maximum observed sorbed inorganic and organic P. Hence, the maximum sorption capacity defines the
545 equilibrium state of sorbed and free-soil P. Moreover, despite the initial representation of the parent material
546 pool in JULES and its depletion through weathering (eq. 43), as the magnitude of changes in the occluded and
547 parent material pools are insignificant over a short-term (20 years) simulation period (Vitousek *et al.*, 1997),
548 these two pools were prescribed using observations. Remaining parameters used to describe soil P fluxes (eqn.s
549 27-44) were prescribed using values from the literature (Table 4).
550
551 We used a combination of data from the *study site* and the nearby K34 site for model evaluation of C fluxes
552 (GPP, NPP) and C pools (soil and vegetation C, leaf, root and wood C) with no calibration of plant and soil
553 organic and soil inorganic P pools included (Table 4).
554
555 **Table 4.** Observations from study site (taken during 2017-2018) and from Manaus site K34 used for model parameterisation
556 and evaluation

Process	Variables	Purpose of use	Reference and site
C associated	GPP	Evaluation	Fleischer et al., 2019, K34
	NPP	Evaluation	Fleischer et al., 2019, K34
	Soil C	Evaluation	Malhi et al., 2009, K34
	CUE	Evaluation	Malhi et al., 2009, K34
	Veg C	Evaluation	Study site
	Leaf C	Evaluation	Study site
	Wood C	Evaluation	Study site
	Root C	Evaluation	Study site
	LAI	Initialisation	Study site
	LMA	Parameterisation	Study site
P associated	Resin	Evaluation	Study site
	Pi Bic	Evaluation	Study site
	Po Bic	Evaluation	Study site
	Po NaOH	Calibration	Study site
	Pi NaOH	Calibration	Study site
	P residual	Parameterisation	Study site
	P HCL	Parameterisation	Study site
	Leaf N	Parameterisation	Study site
	Leaf P	Parameterisation	Study site
	Root P	Parameterisation	Study site
	Plant C:P ratio	Parameterisation	Study site

2.4.1 Model parameterisation and evaluation at test sites

JULES-CNP was parameterised using reported C:P ratios and maximum sorbed organic and inorganic P for each test site (Table 5) as follows:

Table 5. Additional test sites data used for model parameterisation

	AGP-01[a,b]	CAX[a,b]	SA3[a,b]	Gig. Pen. [c]	Hawaii K. [b,d]
$Leaf_{C:P}$	600	600	600	700	691.5
$Root_{C:P}$	1000	1000	1000	1750	1100
$Wood_{C:P}$	3000	3000	3000	5500	5937.5
$Soil_{C:P}$	2000	2000	2000	800	2000
K_{or-max}	0.001	0.001	0.001	0.0033	0.001
K_{in-max}	0.001	0.001	0.001	0.0185	0.001

[a]C:P ratios from Wang, Law and Pak, 2010 and [b]maximum sorbed P capacities from Yang *et al.*, 2014.
[c]Mirabello *et al.*, 2013 [d] C:P ratios from Vitousek, 2004

Model evaluation at test sites, was performed using observed NPP, litterfall, autotropic respiration, biomass and soil C pools taken from different sources. We used NPP and litterfall for the Amazon sites from Aragão *et al.*, (2009) and for Gigante Peninsula from Chave *et al.*, (2003), Hawaii Kokee NPP as reported in Goll *et al.*, (2017) and litterfall as reported in (Yang *et al.*, 2014). Plant respiration was only available at two of Amazon sites (AGP and CAX) (Malhi *et al.*, 2009). The biomass and soil C pools for Amazon sites (CAX and SA3) are taken from Malhi *et al.*, (2009) and biomass from AGP is taken from Jiménez *et al.*, (2009). The Gigante Peninsula biomass is taken from Chave *et al.*, (2003), soil C from Turner et al., (2015), and the Hawaii Kokee C pools are taking as reported in Yang et al., (2014).

2.5 JULES simulations

JULES was first applied at the K34 flux tower site using observed meteorological forcing data from 1999-2019 (Fleisher et a 2019) at half hourly resolution. The following meteorological variables are needed to drive JULES (model inputs) (Best *et al.*, 2011): atmospheric specific humidity (kg kg^{-1}), atmospheric temperature (K), air pressure at the surface (Pa), short and longwave radiation at the surface (W m^{-2}), wind speed (m s^{-1}) and total precipitation (kg m^{-2} s^{-1}). Furthermore, the averaged measured LAI from study site was used to initialise the vegetation phenology module, but was allowed to vary in subsequent prognostic calculations. Soil organic and inorganic sorbed P pools were initialised with study site observations. The JULES-CNP simulations were initialized following the same methodology as in Fleischer et al., (2019), by the spin-up from1850 resulted in equilibrium state (Figure S1). The spin up was performed separately for three versions of JULES (C/CN/CNP) following the same procedure. Furthermore, the transient run was performed for the period 1851-1998 using time-varying CO_2 and N deposition fields. Finally, for the extended simulation period (1999-2019) two runs were performed, the first with ambient the second elevated CO_2 concentrations.

We evaluate the impact of including a P cycle in JULES using three model configurations (JULES C, CN and CNP). We apply JULES in all three configurations using present day climate under both ambient CO_2 and eCO_2. Ambient and eCO_2 were prescribed following Fleischer *et al.*, (2019), with present-day CO_2 based on global monitoring stations, and an abrupt (step) increase in atmospheric CO_2 of +200 ppm on the onset of the transient period (i.e., 1999). However, the comparison period is limited to 2017-18 for which the P measurements are available.

We compare simulated C fluxes (GPP, NPP, litterfall C), C stocks (total vegetation, fine root, leaf, wood, soil) and the CO_2 fertilization effect across model configurations. The CO_2 fertilization effect $\left(CO2_{fert-eff}\right)$ (eq.51) is calculated based on simulated vegetation C under ambient $(VegC\ (aCO_2))$ and eCO_2 $(VegC\ (eCO_2))$ as follows:

$$CO2_{fert-eff} = \frac{(VegC\ (eCO_2) - VegC\ (aCO_2)) \times 100}{VegC\ (aCO_2)}$$ (eq.51)

Furthermore, the net biomass increases due to CO_2 fertilization effect ($\Delta Cveg$) is estimated as follows:

$$\Delta C_{veg} = \Delta BP - \Delta litterfall\ C \qquad\qquad (eq.52)$$

We studied the Water Use Efficiency (WUE) (eq. 53) at half-hourly timestep, then aggregated per month as one of the main indicators of GPP changes (Xiao *et al.*, 2013), and soil moisture content (SMCL), as one of the main controllers of maximum uptake capacity (eq. 27), in order to better understanding the changes in GPP, P demand and uptake as well as excess C fluxes.

$$WUE = GPP/Transpiration \qquad\qquad (eq.53)$$

Moreover, we also estimated the Carbon Use Efficiency (CUE) as an indicator of the required C for the growth (Bradford and Crowther, 2013) as follows:

$$CUE = BP/GPP \qquad\qquad (eq.54)$$

We use JULES-CNP to evaluate the extent of P limitation under ambient and eCO₂ at this rainforest site in Central Amazon. P limitation is represented by the amount of C that is not used to grow new plant tissue due to insufficient P in the system (excess C) (eq. 27). The excess C flux is highly dependent on the plant P and the overall P availability to satisfy demand. We also explore the distribution of the inorganic and organic soil P and their sorbed fraction within the soil layers and under ambient and eCO₂.

2.5.1 Model sensitivity

To test the sensitivity of the P and C related processes to individual model P parameters, six sets of simulations were conducted independently with modified plant C:P stoichiometry (Plant C:P: *SENS1*), P uptake scaling factor (K_P) (Kp: *SENS2*), inorganic (KP_sorb_in: *SENS3*) and organic (KP_sorb_or: *SENS4*) P adsorption coefficients ($K_{sorp-or}$, $K_{sorp-in}$), and maximum inorganic (KP_sorb_in_max: *SENS5*) and organic (KP_sorb_or_max: *SENS6*) sorbed P (K_{or-max}, K_{in-max}). These values were prescribed to vary between ±50% of the observed values and their effect on C pools (plant and soil C) and fluxes (NPP and excess C), and P pools (plant, soil, and soil sorbed P) was assessed. As the derived model parameters from measurements have their own level of uncertainty, we took 50% change to test these parameters at reasonable degree. However, the occluded and weathered P pools are prescribed for this model application, the occluded and weather P coefficients (other two P-related model parameters) were not part of sensitivity tests.

Our model evaluation period is limited to years 2017-18 due to the P measurement availability. However, in order to compare with 15 models studied by Fleischer *et al.*, (2019) we also studied the response of GPP, NPP and BP to eCO₂ for both initial (1999) and 15 years periods (between 1999-2013).

2.5.1   Simulations at test sites

To perform JULES (C, CN, CNP) simulations at test sites we extracted the meteorological input data to drive the model from a global dataset (CRU-NCEP)(Harris *et al.*, 2014) by selecting the closest grid cell to each site when data were not available for a given site (Table 3). Soil texture ancillaries for each site were extracted from a global soil data (HWSD) (Nachtergaele *et al.*, 2010). All simulations were initialised from a global JULES-CN run (Wiltshire *et al.*, 2020) extracted for each site and further spun-up for 2000 years over the 1980-2000 period for the three versions of JULES (C/CN/CNP). Finally, the transient (2000-2013) run was performed using the output of the spin-up for each site.

3.   Results

3.1   Model application under ambient CO₂

3.1.1   Calibration of simulated soil P pools **at *study site***

The maximum sorption capacities (P_{in-max_n}, P_{or-max_n}, eq.37 and 40) were calibrated to the observed P pools. As a result, JULES-CNP could reproduce the measured soil P pools (Fig. 2 and Table 6). Simulated inorganic soil P and sorbed organic and inorganic soil P closely matched the observations (Table 7 and Fig. 2). However, simulated organic soil P overestimates the observations by 60 %.
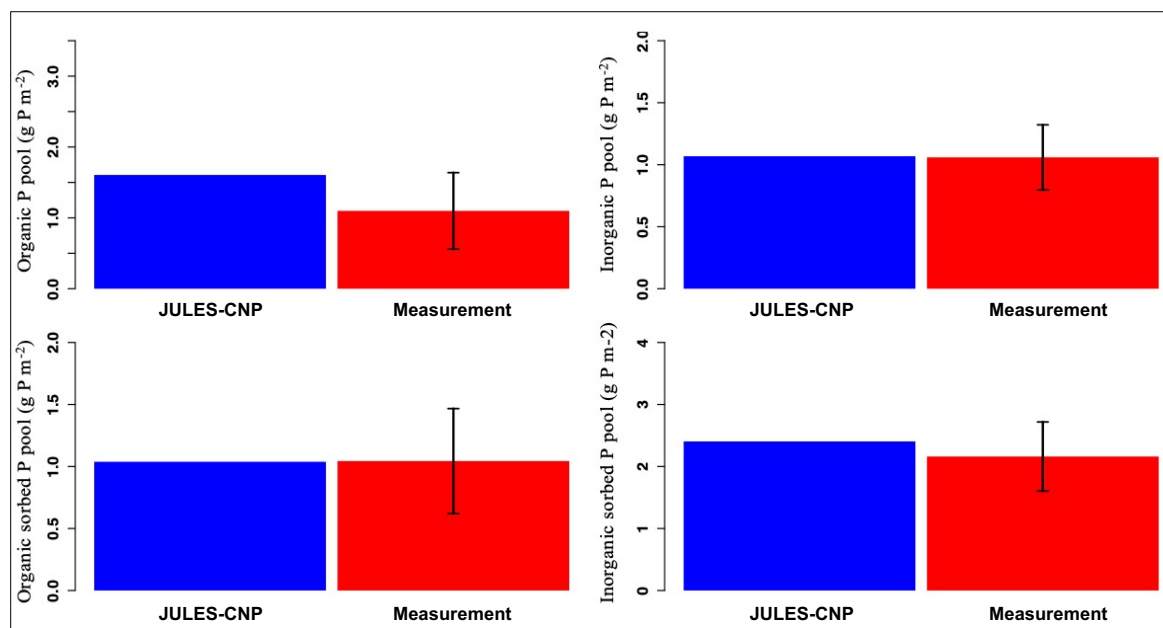
Figure. 2- Modelled vs measured soil phosphorus pools under ambient CO₂ (for the soil depth of 0-30cm). Black line represents standard deviation

Table 6. Observed and simulated phosphorus pools and fluxes. Occluded and weathered P pools were prescribed using the observed values (between period 2017-18).

	Phosphorus pools and fluxes		
	Measured	**Modelled Ambient CO₂**	**Modelled Elevated CO₂**
Organic P (g P m^{-2})	1.09±0.53	1.6	1.57
Inorganic P (g P m^{-2})	1.05±0.33	1.07	0.96
Sorbed organic P (g P m^{-2})	1.04±0.42	1.04	1.03
Sorbed inorganic P (g P m^{-2})	2.1±0.55	2.4	2.4
Occluded P (g P m^{-2})	7.98±2.38	prescribed	prescribed
Weathered P (g P m^{-2})	0.59±12	prescribed	prescribed
Total vegetation P (g P m^{-2})	4.15	4.66	5.11
Soil P – 30cm (g P m^{-2})	13.85	14.7	14.56
Total ecosystem P (g P m^{-2})	-	35.97	35.97
P litter flux (g P m^{-2}yr^{-1})	0.3	0.28	0.29

3.1.2 Model evaluation

JULES-CNP could reproduce the plant and soil C (Figure 2 and Table 7) and N pools and fluxes (Figure S6 and Table 8) under ambient CO_2. Our results show that simulated GPP, is within the range of measurement (3.02 kg C m^{-2} yr^{-1} model vs 3-3.5 kg C m^{-2} yr^{-1} observed, respectively, Table 7).

Simulated NPP, is close to the measured values (NPP: 1.14 - 1.31 observed vs 1.26 modelled kg C m^{-2} yr^{-1}) with autotropic respiration (RESP) also closely following the observations (1.98 observed vs 1.81 modelled kg C m^{-2} yr^{-1}). Biomass production is estimated as a difference between NPP and the amount of C which is not fixed by plants due to the insufficient P in the system (excess C) (eq. 27). The excess C flux depends on the plant P and the overall P availability to satisfy demand (Table 7). The simulated flux of excess C is 0.3 kg C m^{-2} yr^{-1} under ambient CO_2. In JULES-CNP this flux is subtracted from NPP in order to give the BP (eq. 17) (Table 7). Our simulated litterfall overestimates the observations by 32%, however simulated vegetation and its components (fine root, leaf and wood) and soil C stocks match well the observations (Table 7).

Table 7. Observed and simulated carbon pools and fluxes with JULES-CNP (between period 2017-18)

	Carbon pools and fluxes		
	Measured	**Modelled Ambient CO_2**	**Modelled Elevated CO_2**
GPP (kg C m^{-2} yr^{-1})	3.0 – 3.5	3.06	3.9
NPP$_{pot}$ (kg C m^{-2} yr^{-1})	-	1.27	1.77
Plant respiration (kg C m^{-2} yr^{-1})	1.98	1.78	2.12
Excess C flux (kg C m^{-2} yr^{-1})	-	0.30	0.81
Biomass Production (kg C m^{-2} yr^{-1})	1.14±0.12	0.96	0.94
Litter C flux (kg C m^{-2} yr^{-1})	0.69±0.15	0.91	0.83
Leaf C (kg C m^{-2})	0.37±0.2	0.38	0.40
Wood C (kg C m^{-2})	22.01	22.4	24.71
Root C (kg C m^{-2})	0.37±0.2	0.38	0.40
Vegetation C (kg C m^{-2})	22.75±0.3	23.16	25.52
Soil C stock (kg C m^{-2})	12.7	13.2	12.71
LAI (m^2 m^{-2})	5.6±0.36	5.77	6.12

3.1.3 Comparison of JULES C, CN and CNP under ambient CO_2 at *study site*

We compare simulated C pools and fluxes from JULES-C, JULES-CN and JULES-CNP (Figure 3). There is no difference between C stocks and fluxes in simulations from JULES C and CN indicating that there is no N limitation at this tropical site in the CN simulations. However, simulated BP and litter flux of C by JULES C/CN are higher than in JULES-CNP but also overestimate the observations (litter flux of JULES C/CN: 1.18, JULES-CNP: 0.91 and obs 0.69 (kg C m^{-2} yr^{-1}) and BP of JULES C/CN: 1.24, JULES-CNP: 0.96 and obs 1.14-1.31 (kg C m^{-2} yr^{-1}), respectively). By including P cycling in JULES an excess C flux of 0.3 (kg C m^{-2} yr^{-1}) is simulated, indicating a 24% P limitation to BP at this site according to JULES-CNP, which represents a 29% decrease in BP compared to JULES-C/CN. Consequently, the total vegetation C stock for models without P inclusion is higher than the CNP version (+3% difference) due to the lack of representation of P limitation. The simulated soil C stock in JULES C and JULES CN is also higher than in the CNP version (JULES C/CN: 13.93 vs. JULES-CNP: 13.18 (kg C m^{-2} yr^{-1})) and higher than the observations. Moreover, CUE in JULES C/CN (eq.54) is higher than observations and JULES-CNP (JULES C/CN: 0.38 vs. JULES-CNP: 0.31, obs: 0.34 ±0.1(dimensionless).
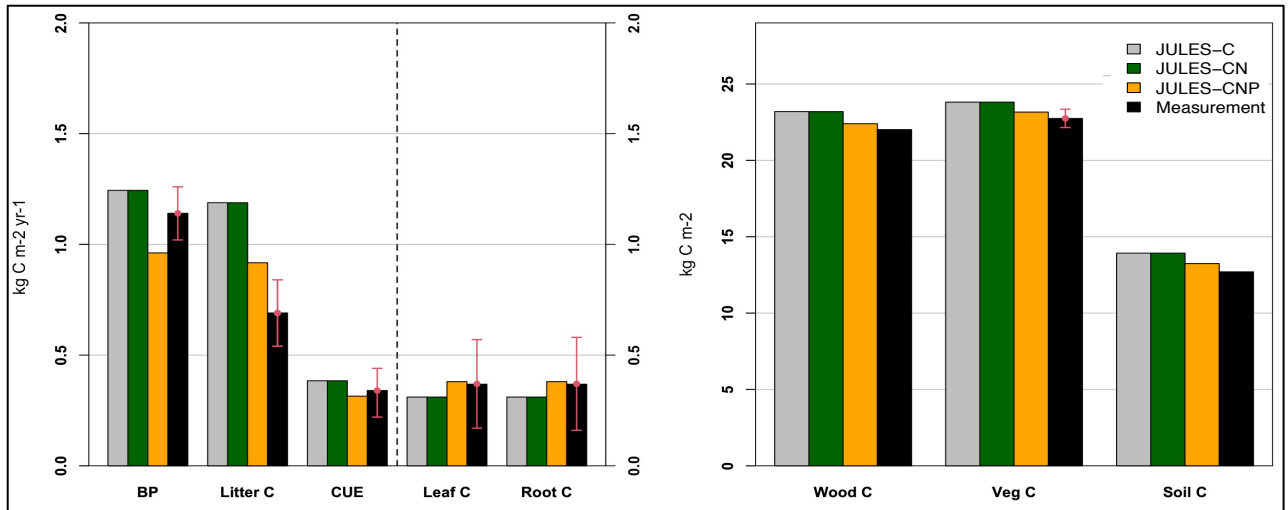
Figure. 3- JULES C, CN, CNP modelled vs measured C pools (Leaf, root, wood, Veg and Soil C) (in kg C m^{-2}) and fluxes (BP and Litter C) (in kg C m^{-2} yr^{-1}) and CUE under ambient CO_2. Note that CUE is unitless.

3.1.4   Model evaluation at test sites under ambient CO_2

Evaluation of JULES C, CN and CNP at five test sites against the observed C pools and fluxes demonstrate that the inclusion of P processes improved the simulation of C pools and fluxes across all test sites (Figure 4). At all Amazon sites JULES C and CN overestimated BP compared to JULES-CNP which estimated lower BP values which were closer to the measurements for AGP (JULES-C: +35%, JULES-CN: +33%; JULES-CNP: +21%), CAX (JULES-C: +45%, JULES-CN: +44%; JULES-CNP: +7%) and SA3 (JULES-C: +27%, JULES-CN: +26%; JULES-CNP: -23%). Moreover, at Gigante Peninsula the C and CN versions overestimated BP (+42% and +40%, respectively), and CNP slightly underestimated BP (-15%). Furthermore, at the Hawaii Kokee site, all three versions of JULES underestimated the BP (C:-8%, CN:-8%, CNP: -32%). The litterfall and respiration fluxes in JULES-CNP have decreased compared to the JULES C and CN versions which overestimated both fluxes at all the test sites compared to the measurements. The litterfall flux comparisons show a significant overestimation using JULES C and CN versions across all the tested sites. Along the Amazon sites inclusion of P limitation reduced the litterfall flux but still overestimated (AGP: +50%, CAX: +24% and SA3: +16%) and at Gigante Peninsula and Hawaii Kokee slightly underestimated (Gigane Peninsula: -9% and Hawaii Kokee -19%). The respiration measurements were only available at two Amazon sites (CAX and SA3) at which inclusion of P limitation resulted in a well estimated flux at both sites compared to the JULES C/CN versions (CAX site: C-only: +38%, CN: +38%, CNP: -1%; SA3 site: C-only: +38%, CN: +38%, CNP: -2%).

The total vegetation biomass also reduced using JULES-CNP compared to the other versions and yield closer values to the measurements across all the sites. However, except at the AGP site in which all three versions of JULES slightly underestimated the biomass (C: -1%, CN: -1%, CNP: -6%), at the other test sites JULES-CNP estimated lower biomass pools compared to the other versions which overestimated total vegetation biomass. Similarly, the soil C pool was overestimated prior to P limitation inclusion in JULES at the test sites, and the JULES-CNP estimated a closer value compared to the measurements (slight underestimation at CAX and SA3 sites: -5% and -18% respectively, and close values at Gigante Peninsula and Hawaii Kokee: +3% and +4%, respectively).
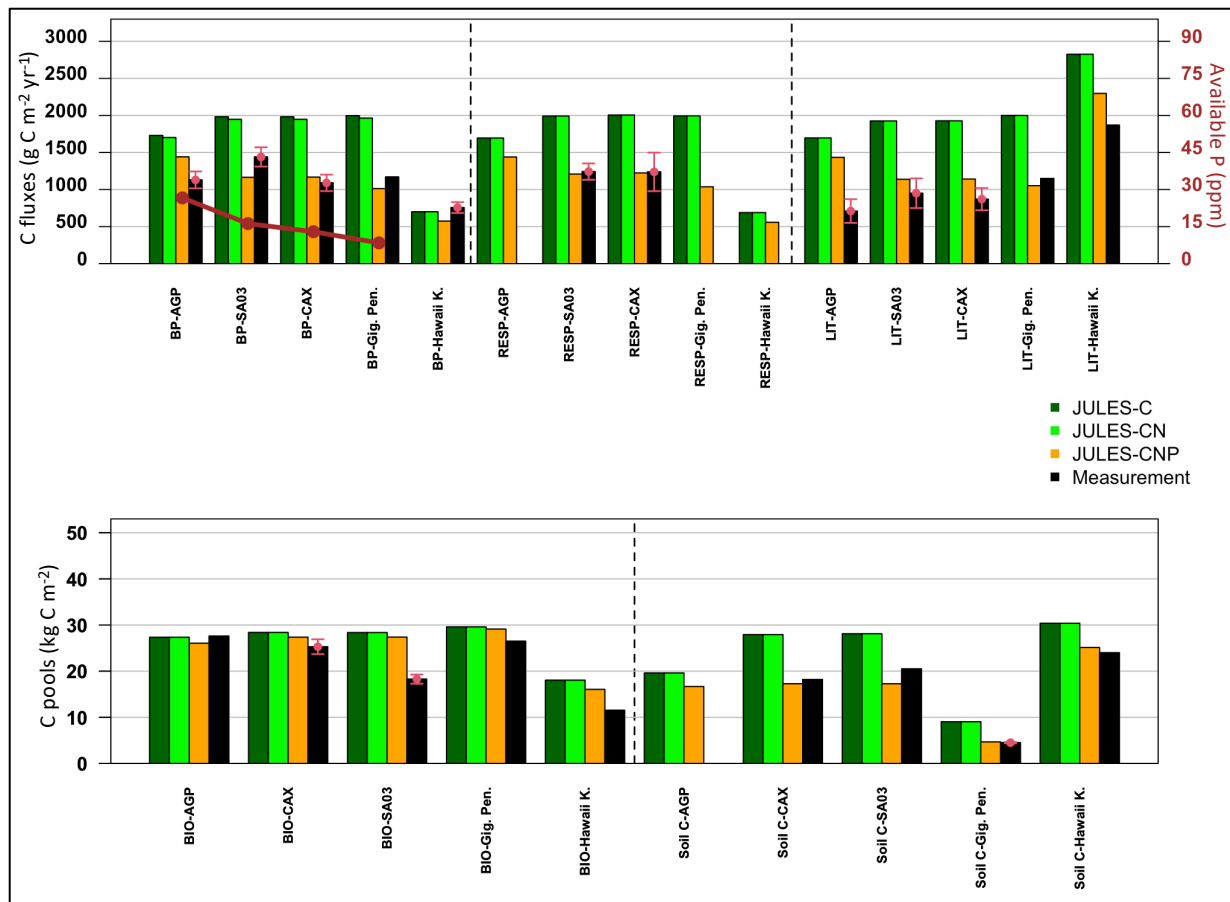
Figure. 4- Observed and simulated (JULES C, CN, CNP) C fluxes and pools (averaged measurements: red points, sd: red arrows) and available observed P (dark red points and lines (reported in ppm)) at test sites across the Amazon (AGP, SA03, CAX), Gigante Peninsula (Gig. Pen.) and Hawaii Kokee (Hawaii K.).

3.1.5 Model sensitivity

The results indicate that among all the corresponding C and P pools and fluxes, the excess C flux – which demonstrates P limitation to growth – shows the highest sensitivity to changes in C:P ratios (Figure 5-a), K_P (Figure 5-b), and K_{or-max} (Figure 5-c) and K_{in-max} (Figure 5-d). A decrease in plant C:P results in a large increase in excess C. This is due to the higher plant P demand as a result of lower plant C:P ratios. An increase in the uptake factor and maximum sorbed organic and inorganic P also results in an increase in excess C. This is due to the higher uptake demand through higher uptake capacity (due to higher K_P) and lower available P for uptake due to higher organic and inorganic sorbed P (due to higher K_{or-max}, K_{in-max}). Since the total P in the system is lower than the plant demand, the uptake capacity and sorbed P, higher P limitation is placed on growth (decreasing BP) which results in an increase in excess C and decrease in plant C, but also soil C which is a result of lower litter input (Figure 5). Total soil P shows low sensitivity to changes in plant C:P and uptake factor but high sensitivity to maximum inorganic sorbed P. Moreover, sorbed P shows middle to high sensitivity to maximum organic and inorganic sorbed P respectively (Figure. S5). Nevertheless, organic and inorganic P adsorption coefficients ($K_{sorp-or}$, $K_{sorp-in}$) show no sensitivity to C and P pools and fluxes. This is due to limiting the organic and inorganic P sorption terms to be controlled only by maximum sorption capacity, hence no effect applied by organic and inorganic adsorption coefficients.
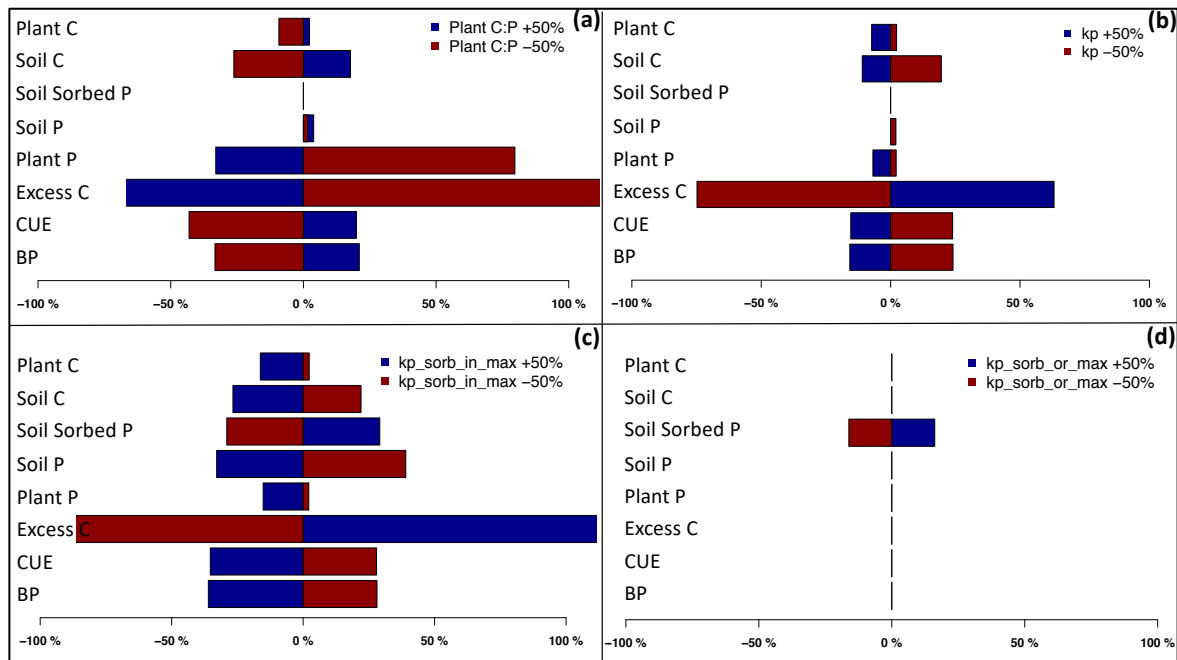
Figure. 5- Sensitivity of C and P pools to variation in key model parameters: prescribed tissue C:P (a), Kp(b), Kp_sorb_ in(c), Kp_sorb_ or(d) under ambient CO_2.

3.2 Model application under elevated CO_2

3.2.1 Simulated plant and soil C and P pools and fluxes -JULES-CNP: eCO₂ vs ambient CO₂

The eCO₂ simulation using JULES-CNP yields a higher GPP compared to the ambient CO_2 (0.83 (kg C m^{-2} yr^{-1}) increase), as a result of CO_2 fertilization. Moreover, due to the GPP increase, NPP and RESP also increased compared to ambient CO_2 (NPP: 0.49 and RESP:0.3 (kg C m^{-2} yr^{-1}) increase) (Table 7). The total simulated vegetation C pool increases under eCO₂ compared to ambient CO_2 (0.41 kg C m^{-2}), hence the estimated plant P (estimated as a fraction of C:P ratios) increases as well (+0.45 (g P m^{-2})) (Fig. 6, Table 6). Thus, the simulated plant P demand is higher, and as the total available soil P for uptake is limited, the simulated excess C flux increases to 0.51(kg C m^{-2} yr^{-1}). Moreover, despite the higher NPP under eCO₂ compared to simulated NPP under ambient CO_2, due to the substantial increase in simulated excess C, the BP is similar to the ambient CO_2 (2% difference).

The simulated organic soil P under eCO₂ were close to those under ambient CO_2 (1.6 g P m^{-2}) (Table 7). This is due to the same parameterization of the output fluxes from this pool for eCO₂ and ambient CO_2. The simulated pool of inorganic P under eCO₂ decreases compared to the ambient CO_2 by 0.11 (g P m^{-2}) due to the increased plant P pools and slight increase in uptake (+0.13 %).
However, the simulated sorbed organic and inorganic soil P from eCO₂ are similar to those simulated under the ambient CO_2 which is due to the same parameterization of sorption function (maximum sorption capacity) from the ambient CO_2 run as explained in calibration section. Moreover, the modelled occluded and weathered soil P were similar to those in the ambient CO_2 simulation (Table 7) which is due to the same prescribed observational data that was used for this simulation.

3.2.2 Comparison of JULES C, CN and CNP under elevated CO_2

JULES C/CN show higher vegetation and soil C pools, BP and litter flux compared to JULES-CNP: (Table 8, Figure. S2). Under eCO₂, simulated NPP using JULES C-CN is 4.5% higher than JULES-CNP and the BP with JULES- C/CN is 96.8% higher than in JULES-CNP which simulates an excess C flux of 0.81 (kg C m^{-2} yr^{-1}) equivalent to 46% P limitation under eCO₂. As a result of P limitation and eCO₂, the simulated CO_2 fertilization effect estimated based on changes in biomass under ambient and eCO₂ was reduced from 13% with JULES-C/CN to 10% JULES-CNP. Moreover, the CUE from JULES C/CN is 87.5% higher than the JULES-CNP as a result of high P limitation over biomass production.

815 **Table 8.** Simulated C pools and fluxes with JULES C/CN and difference in percentage with JULES-CNP model under
816 eCO₂. A positive % means larger respective values simulated with JULES C and JULES CN than with JULES-CNP
817 (between period 2017-18).

	GPP	NPP	BP	CUE	Litter C	Leaf C	Root C	Wood C	Soil C
JULES C/CN	4.1	1.85	1.85	45%	1.77	0.42	0.42	26.1	19.2
JULES-CNP	3.9	1.77	0.94	24%	0.83	0.4	0.4	24.71	12.71
ΔC/CN: CNP	5.1%	4.5%	96.8%	87.5%	113.3%	5%	5%	5%	51.1%

3.2.2.1 Inter-models under elevated CO₂

Following Fleischer *et al.*, (2019), we report the simulated response to eCO₂ for year 1999 (initial: CO₂ effect) and 1999-2013 (15 years: final effect) which are different than our evaluation period (2017-18). Using JULES-C and JULES-CN under eCO₂, simulated GPP and NPP during the 1ˢᵗ year increase by 30% and 61% respectively and by 28% and 52% after 15 years (Figure. 6). However, using JULES-CNP, eCO₂ increases simulated GPP, NPP and BP responses during the 1ˢᵗ year by 29%, 51% and 20% and by 28%, 43% and 7%, after 15 years, respectively.

Corresponding simulated CUE during the 1ˢᵗ year and 15 years shows an increase of 24% and 20% in response to eCO₂ using JULES C/CN, respectively. However, using JULES-CNP, simulated CUE for the 1ˢᵗ and after 15 years is reduced by 7% and17% in response to eCO₂.

Simulated total biomass (leaf, fine root and wood C) (ΔC*veg*) using JULES- C/CN for the 1ˢᵗ and 15 years of eCO₂ increased by 9% and 13% respectively. However, using JULES-CNP ΔC*veg* only increases by 0.5% and 9% for 1ˢᵗ and 15 years of eCO₂, respectively.
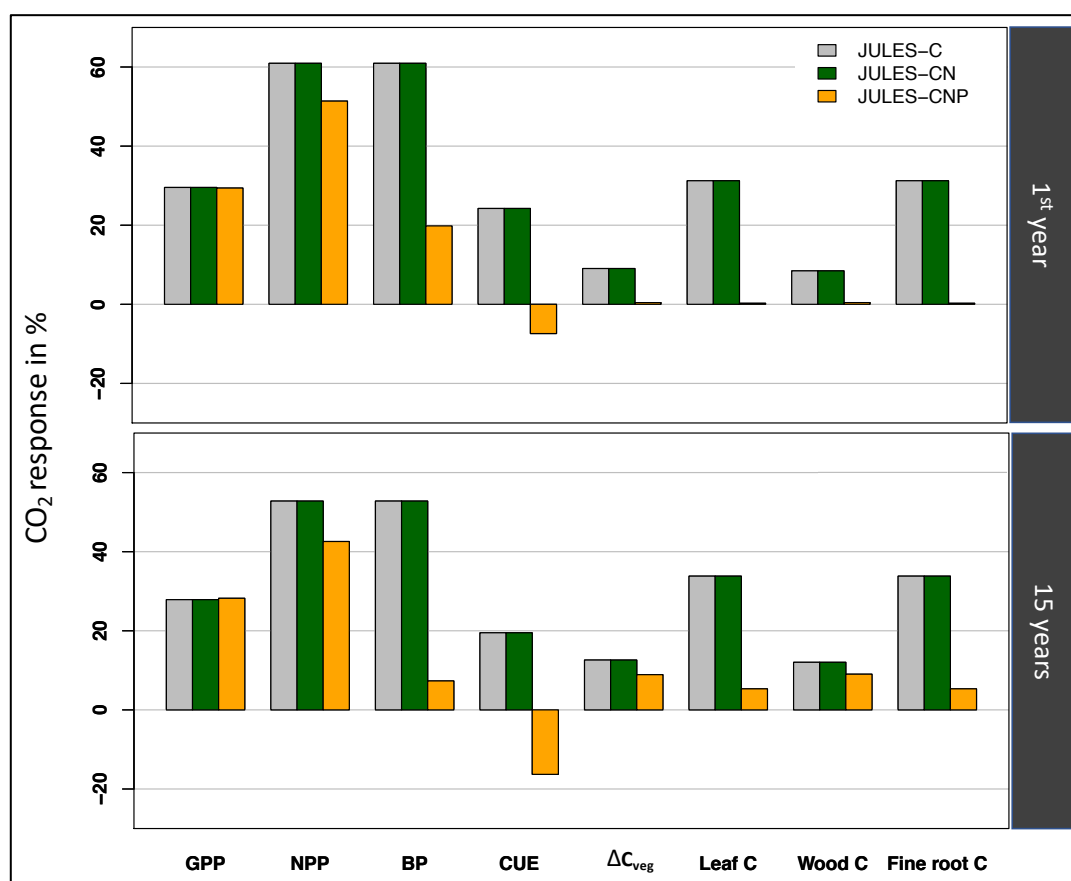
Figure. 6- Relative effect of eCO₂ on simulated GPP, NPP, BP, CUE, ΔC*veg*, leaf C, wood C and fine root C, using three versions of JULES model in 1ˢᵗ (initial response) and 15 years periods (final response).

3.3 Plant P Demand, uptake and excess C under ambient and elevated CO_2

To understand further the CP-cycle dynamics, we studied the monthly averaged plant P demand and the relative (limited) P uptake (eq. 26) under both ambient and elevated CO_2 conditions (Figure. 7).

Under ambient CO_2 condition the highest GPP is estimated at 0.29 ± 0.016 kg C m^{-2} month^{-1} in July and the lowest at 0.17 ± 0.051 kg C m^{-2} month^{-1} in October (Figure. 7-a). The estimated WUE and SMCL in October is among the lowest estimated monthly values at 2.3 ± 0.51 kg CO_2/kg H_2O and 526.2 ± 31 kg m^{-2} respectively (Figure. 7-c). The highest P demand is estimated at 0.4 ± 0.02 g P m^{-2} month^{-1} in July and the lowest demand at 0.2 ± 0.08 g P m^{-2} month^{-1} in October. Consequently, the highest and lowest uptake (0.32 ± 0.01 and 0.19 ± 0.07 g P m^{-2} month^{-1}, respectively). The excess C for the highest and lowest GPP and demand periods are estimated at 0.4 ± 15 and 0.04 ± 0.07 kg C m^{-2} month^{-1}, respectively.

However, similar to ambient CO_2, under eCO_2 condition the highest estimated GPP is in July at 0.36 ± 0.017 kg C m^{-2} month^{-1} and lowest for October 0.25 ± 0.062 kg C m^{-2} month^{-1} (Figure. 7-b). The estimated WUE and soil moisture content (SMCL) for the lowest GPP period is among the lowest monthly estimated values at 3.5 ± 0.74 kg CO_2/kg H_2O and 552 ± 33 kg m^{-2} for October respectively (Figure. 7-d). The highest P demand is estimated for July at 0.51 ± 0.02 g P m^{-2} month^{-1} with the uptake flux of 0.31 ± 0.02 g P m^{-2} month^{-1} and the lowest demand is estimated for October at 0.32 ± 0.1 g P m^{-2} month^{-1} with the estimated uptake flux of 0.26 ± 0.06 g P m^{-2} month^{-1}. The highest excess C flux is also for July at 1.01 ± 0.17 kg C m^{-2} month^{-1} and lowest for October 0.27 ± 0.29 kg C m^{-2} month^{-1}, respectively.

However, despite the P limitation in both eCO_2 and ambient CO_2 conditions, the P uptake flux under eCO_2 is higher than the ambient CO_2 condition. This is due to the higher WUE and increased SMCL (controlling uptake capacity (eq. 27)) under eCO_2 condition, hence more water availability during the dry season to maintain productivity and critically transport P to the plant (see eq. 27), compared to ambient CO_2 condition (Figure. 7-c and d). Additionally, in JULES both the vertical discretisation (Burke, Chadburn and Ekici, 2017) and mineralisation terms (Wiltshire *et al.*, 2021) depend on the soil moisture and temperature. Thus, higher P concentration and uptake under eCO_2 condition.
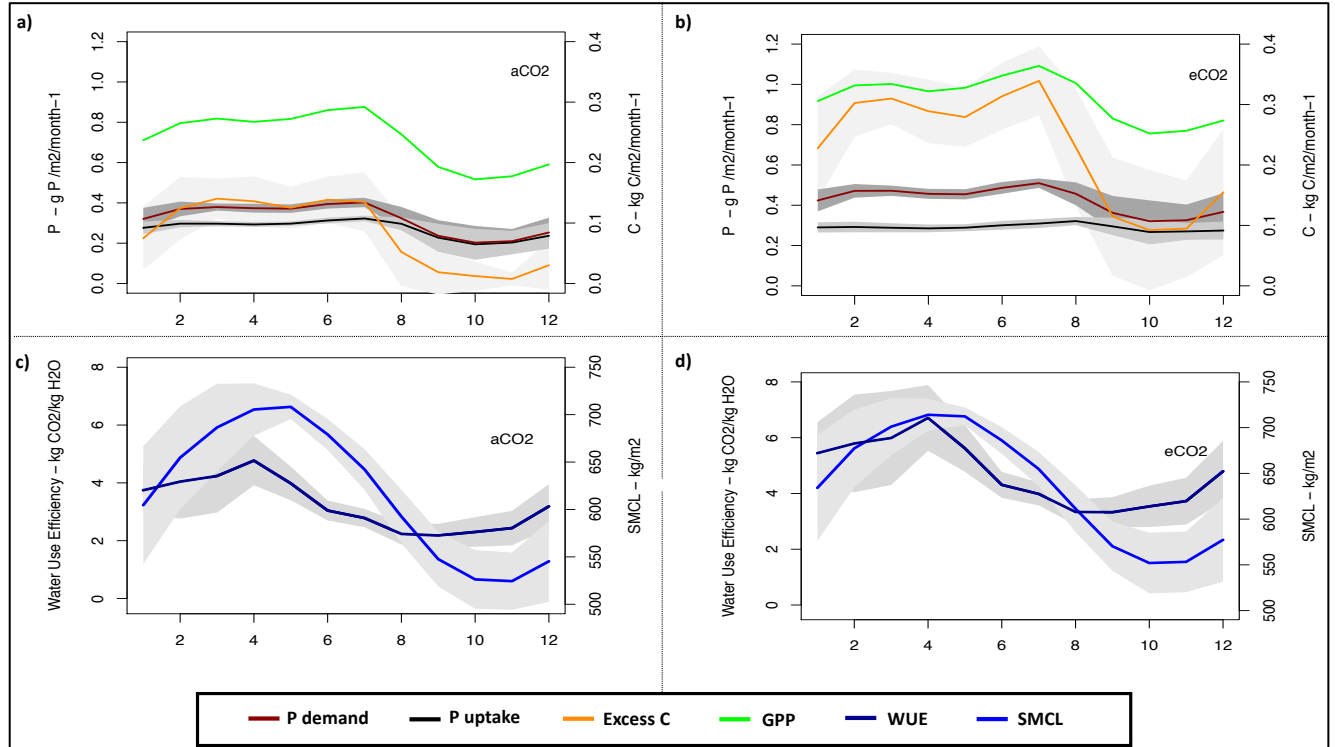
Figure. 7- Simulated monthly plant P demand and uptake (g P m^{-2} month^{-1}), excess C and GPP (kg C m^{-2} month^{-1}) under a) aCO_2 and b) eCO_2, water use efficiency (g m^{-2} month^{-1}) under c) ambient CO_2 (aCO_2) and d) eCO_2 conditions. The grey area represents the standard deviation.

3.4 Soil P pools profile under ambient CO₂ and elevated CO₂

We explored the distribution of the inorganic and organic soil P and their sorbed fraction within the soil layers and under different CO_2 conditions (Figure. S3). Both the ambient and eCO_2 simulations have a close inorganic soil P distribution at the topsoil layer (0-30cm) (0.85 vs. 0.9 (g P m^{-2}) respectively) as well as similar organic soil P distribution (0.85 vs 0.9 (g P m^{-2}) respectively).

However, the organic soil P and sorbed forms of inorganic and organic soil P profiles are not changing significantly between different sets due to the similar parameterization of the processes that control these pools (processes which are related to the physical aspects of soils, hence not changing under eCO_2 condition) and the same parameter values used for both ambient and eCO_2 runs.

Moreover, the soil P within 30cm soil depth for ambient and eCO_2 conditions is at 14.7 (g P m^{-2}) and 14.56 (g P m^{-2}) respectively, and the total ecosystem P for both ambient and eCO_2 conditions is at 35.97 (g P m^{-2}). However, the slightly lower soil P in the eCO_2 condition is due to the higher plant P demand compared to the ambient condition, hence the higher allocated P vegetation (10%) under eCO_2 condition.

4. Discussion

Studies show the significant role of the tropical forests, and Amazonia in particular, in C uptake and regulating atmospheric CO_2 (Brienen *et al.*, 2015; Phillips *et al.*, 2017). As soil P availability is low in the majority of Amazonia (Quesada *et al.*, 2012), the competition for nutrients by both plant and soil communities is high (Lloyd *et al.*, 2001). The responses of these communities to eCO_2 under P limited conditions remains uncertain (Fleischer *et al.*, 2019). These responses in P enabled models are represented in different ways regarding the excess C which is not used for plant growth due to P limitation. Either growth is directly downregulated taking the minimum labile plant C, N and P (Goll *et al.*, 2017), or photosynthesis is downregulated via V_{cmax} and J_{max} (Comins and McMurtrie, 1993; Yang *et al.*, 2014; Zhu *et al.*, 2016) and models like JULES-CNP downregulate NPP via respiration of excess carbon that cannot be used for growth due to plant nutrient constraints (Haverd *et al.*, 2018). The estimated CUE depends on the modelling approach. Models that down regulate the photosynthetic capacity and GPP consequently (Comins and McMurtrie, 1993; Yang *et al.*, 2014; Zhu *et al.*, 2016) simulate a positive CUE response to CO_2 fertilization while models that down regulate the NPP and respire the excess C (Haverd *et al.*, 2018) simulate a negative CUE response (Fleischer *et al.*, 2019) which is in line with field studies showing lower CUE when nutrient availability declines (Vicca *et al.*, 2012b). However, this remains a major uncertainty in understanding the implication of P limitation on terrestrial biogeochemical cycles.

The JULES-CNP structure represent key P processes in both plant and soil pools and can be applied to the Amazon region using existing soil (Quesada *et al.*, 2011) and foliar structural and nutrient (Fyllas *et al.*, 2009) data for parameterisation. The model can be applied globally and under future climate projections using global soil P data (Sun *et al.*, 2021) for model initialization and PFT-specific plant (Zechmeister-Boltenstern et al. 2015) and soil stoichiometries (Zechmeister-Boltenstern et al. 2015; Tipping et al. (2016), sorption and weathering ratios (based on lithological class specific from the GliM lithological map (Hartmann and Moosdorf, 2012) and soil shielding from Hartmann et al., (2014)).

4.1. Evaluation of model performance

At the study site, JULES-CNP could reproduce the magnitude of soil organic and inorganic P pools and fluxes. The relative distribution of total organic P, total inorganic P and residue P fractions of total P in soils under Brazilian Eucalyptus plantations (Costa *et al.*, 2016) shows inorganic P fraction of 28% from total soil P which is close to our estimation of 24% and organic P fraction of 30% from total soil P which is higher than our estimated fraction of 18%. Thus, we may need to improve the process representation or parameters that control the organic P concentration, such as litter flux and decomposition, soil organic P mineralization, and immobilization in the future.

Our estimated maximum P uptake, which represents the actual available P for plant uptake (Goll *et al.*, 2017), for both ambient and eCO_2, is highly correlated with the plant P demand ($R^2 = 0.96$ and 0.52 respectively). The plant P demand depends on the GPP changes which are reflected by the WUE (Hatfield and Dold, 2019). Hence, under ambient CO_2, JULES-CNP simulates lower GPP and plant P demand during the dry season than during the wet season. Sufficient P uptake during these periods results in the lowest P limitation, thus the lowest simulated excess C. Nevertheless, under eCO_2 the same pattern is simulated but a higher availability of soil P due to the stomatal closure in the dry season. Hence, due to the plant's more efficient water usage, the soil

moisture in the dry season is higher (Xu *et al.*, 2016) which impacts our capped P uptake flux (eq. 27) and increases the uptake capacity respectively.

Overall, JULES-CNP reproduced the observed C pools and fluxes which are in the acceptable ranges compared to the measurements. However, using the JULES default V_{cmax} estimation method (eq. 40), the model slightly underestimates the total GPP (2.9 kg C m^{-2} yr^{-1} vs. 3-3.5 kg C m^{-2} yr^{-1}). Therefore, in this version of the model, we used the improved V_{cmax} estimation method based on N and P (eq. 46) which resulted in a final estimated GPP closer to the measurements (3.06 kg C m^{-2} yr^{-1}).

Our results show an increase in GPP (21%) in response to eCO$_2$ which is higher than the average increase of GPP reported in mature eucalyptus forests (11%), also growing under low P soils at the free air CO$_2$ enrichment experiment (EucFACE) facility in Australia (Jiang *et al.*, 2020). This can be related to the lower decrease of biomass growth response estimated by JULES-CNP (-3%) compared to the measurements from mature eucalyptus forests (-8%) (Ellsworth *et al.*, 2017), due to the P limitation which was shown to impact the above-ground biomass growth response in mature forests (Körner *et al.*, 2005; Ryan, 2013; Klein *et al.*, 2016).

In order to estimate the biomass production (BP), we deducted the excess C fluxes from NPP. Using JULES C/CN models, the simulated biomass productivity enhancement due to eCO$_2$ (49%) is in the middle range of the reported for different biomes by Walker *et al.*, (2021). Moreover, our estimated difference of BP between ambient and eCO$_2$ conditions (2%) is close to the estimated difference for mature forests (3%) (Jiang *et al.*, 2020).

A global estimation for tropical forests using the CASA-CNP model which includes N and P limitations on terrestrial C cycling, shows that NPP is reduced by 20% on average due to the insufficient P availability (Wang, Law and Pak, 2010) which is close to our estimated P limitation of 24%. This finding is in line with a field study that shows a strong correlation between the total NPP and the soil available P (Aragão *et al.*, 2009). The estimated decrease of NPP in response to eCO$_2$ as a result of P limitation is in line with the findings from CLM-CNP model at five tropical forests (Yang *et al.*, 2014) which indicates the CO$_2$ fertilization dependency on the processes that affect P availability or uptake.

Our estimated CUE (0.31) is close to that by Jiang *et al.* (2020) for mature eucalyptus forests (0.31±0.03), as well as to the measurement for our study site (0.34 ±0.1). There is currently a lack of representation of stand age in JULES-CNP which can significantly affect CUE (e.g. mature trees are less responsive to the nutrient limitations) (De Lucia *et al.*, 2007; Norby *et al.*, 2016). However, a recent development of Robust Ecosystem Demography (RED) model in JULES (Argles *et al.*, 2020) and its integration into JULES-CNP in the future can address this issue.

Under low P availability, all available P is considered to be adsorbed or taken by plant and microbes for further consumption, with leaching considered to be minor within the time scales of our study period (Went and Stark, 1968; Bruijnzeel, 1991; Neff, Hobbie and Vitousek, 2000). Despite studies that show the possibility of P fixation as a source of available P for plants (Van Langenhove *et al.*, 2020; Gross *et al.*, 2021), due to the strong fixation of P in the soil (Aerts & Chapin, 2000; Goodale, Lajtha,Nadelhoffer, Boyer, & Jaworski, 2002), the P deposited is unlikely to be available to plants in the short term (de Vries et al., 2014), for this reason this version of JULES-CNP did not include P deposition. However both P deposition and leaching are likely to have a very important role on sustaining the productivity of tropical forests in the Amazon over longer time scales (Van Langenhove *et al.*, 2020) and needs to be considered in future studies. Moreover, biochemical mineralisation is also not included in the current version of JULES-CNP which only accounts for total mineralization. However, models that include this process show no significant difference between total and biochemical mineralized P which can be due to complexity of identifying the inclination of mineralization versus uptake (Martins *et al.*, 2021). Lastly, in order to capture plant internal nutrient impact on the C storage, future work should focus on implementing recent developments including Non-Structural Carbohydrate pools (NSC) (Jones *et al.*, 2020) in JULES-CNP.

4.1.1. Evaluation of model performance at test sites

Overall, inclusion of P processes in JULES-CNP improved the previously overestimated C fluxes and pools using JULES-C and -CN versions. Generally, the biomass productivity tends to follow the observed P availability (Figure 4), where the sites with higher available P for uptake simulated higher productivity which is in line with observations across P availability in the Amazon (Aragão *et al.*, 2009). Nevertheless, this tendency could be altered if the natural conditions in these forests are perturbated. For instance, in case of the high mortality events in these P limited sites (Malhi *et al.*, 2009; Pyle *et al.*, 2009), regrowing forests developing over the highly weathered oxisols with limited available P (Davidson *et al.*, 2004), results in the shifting limitation from P to N (Herbert, Williams and Rastetter, 2003). Hence, the controlling processes under N limitation will be N-related and processes such as N leaching or outgassing (Yang *et al.*, 2014) will define the productivity. This shifting in limitation condition is not represented by JULES-CNP, therefore at few tested sites the model overestimated the P limitation, thus underestimated the productivity below the measured values. Moreover, the higher (than other sites) BP in JULES C/CN at the the Gigante Peninsula is related to the higher solar radiation in the forcing data at this site (Figure S8).

The estimated litterfall and respiration fluxes were considerably lower with JULES-CNP than JULES-C and -CN due to the lower simulated NPP with the former in closer agreement with the observations at all sites. Consequently, the total vegetation and soil C pools have lower values under the P limitation (Malhi *et al.*, 2009), which could not be captured by JULES-C and -CN and successfully represented by JULES-CNP.

As shown in Figure 5, JULES-CNP is highly sensitive to the five parameters needed to run JULES-CNP in addition to JULES-C and JULES-CN which were prescribed for simulations at test sites. The successful model performance at these sites demonstrates the importance of these parameters in JULES-CNP with implications for global scale simulations.

4.2. Inter-models Comparison of JULES C, CN and CNP

The comparison of simulated GPP enhancement across JULES versions for the 1st year is within the middle range of the 1st year CO_2 responses of the C/CN models studied by Fleischer *et al.*, (2019) evaluating simulated eCO_2 effects at a site in Manaus using the same meteorological forcing and methodology used in this study for a range of DGVM's. However, comparison for 15 years of eCO_2, shows that the simulated response with JULES-CNP is on the higher end of Fleischer *et al.*, (2019) study which is due to the higher estimated biomass growth by JULES-CNP (Table S1). Similarly, using JULES-CNP our estimated GPP enhancement is on the higher end of model estimations in Fleischer *et al.*, (2019). Moreover, comparing the GPP responses between different versions of (JULES C/CN and CNP), the JULES-CNP shows a slightly higher response to CO_2 fertilization associated with the higher WUE changes (Xiao *et al.*, 2013) (Figure. S4). This is due to the higher sensitivity of the plant to water availability than P availability in the P limited system (He and Dijkstra, 2014). Hence, under eCO_2 due to water-saving strategy of plants and stomatal closure (Medlyn *et al.*, 2016), simulated transpiration is decreased (Sampaio *et al.*, 2021) and photosynthesis is enhanced compared ambient CO_2 .

To that end, the monthly changes of WUE in JULES-CNP are highly correlated to the GPP, hence the lowest and highest WUE follow the same periods as GPP similar to responses captured with models studied by Fleischer *et al.*, (2019) (Table. S1).

Our estimated NPP enhancement using JULES C/CN models for both 1st and 15 years period is within the middle range of the models in Fleischer *et al.*, (2019). Nevertheless, JULES-CNP response of BP is in the lower band of the CNP models in Fleischer *et al.*, (2019) and close to the estimations from CABLE (Haverd *et al.*, 2018) and ORCHIDEE (Goll *et al.*, 2017) models, which may be due to the similar representation of P processes and limitation between these models. However, our results show a 29% decrease in NPP using JULES-CNP compared to JULES-C/CN which is smaller than the differences between the CLM-CNP and CLM-CN versions (51% decrease) (Yang *et al.*, 2014). The lower estimated decrease in JULES highlights the need to further study the fully corresponding plant C pools and fluxes to the changes in soil and plant P. Therefore, future work should be focused on the improvement of the total P availability and the plant C feedbacks. Moreover, there are other environmental factors such as temperature which shows a possible impact on the CO_2 elevation and the changes of NPP (Baig *et al.*, 2015) which needs further improvement in our model.
The CUE estimations of 1st year and 15 years response to CO_2 elevation from JULES C/CN are in the middle range of C/CN models in Fleischer *et al.*, (2019). However, the estimated CUE using JULES-CNP for 1st and 15 years are in the low range of CNP models reported by Fleischer *et al.*, (2019) which is due to the same reason discussed for NPP comparison.

1059 Finally, our estimated total biomass enhancement ($\Delta C veg$) using JULES C/CN for the 1st and 15 years are in the
1060 middle range of C/CN models from Fleischer *et al.*, (2019) and in lower range of CNP models from Fleischer *et*
1061 *al.*, (2019) using JULES-CNP. Nevertheless, while JULES-CNP includes the trait-based parameters (Harper *et*
1062 *al.*, 2016), other functions such as flexible C allocation and spatial variation of biomass turnover are still
1063 missing and future model improvement should be focused on their inclusion.
1064
1065 **5. Conclusion**
1066
1067 Land ecosystems are a significant sink of atmospheric CO_2, ergo buffering the anthropogenic increase of this
1068 flux. While tropical forests contribute substantially to the global land C sink, observational studies show that a
1069 stalled increase in carbon gains over the recent decade (Brienen *et al.*, 2015; Hubau *et al.*, 2020). However
1070 modelling studies that lack representation of P cycling processes predict an increasing sink (Fernández-Martínez
1071 *et al.*, 2019; Fleischer *et al.*, 2019). This is particularly relevant for efforts to mitigate dangerous climate change
1072 and assumptions on the future efficacy of the land C sink. Therefore, in this study, we presented the full
1073 terrestrial P cycling and its feedback on the C cycle within the JULES framework. Our results show that the
1074 model is capable of representing plant and soil P pools and fluxes at a site in Central Amazon and across the
1075 extended P limited test sites in Amazon, Gigante Peninsula and Hawaii chronosequence provided with site level
1076 data for model parameterisation. Moreover, the model estimated a significant NPP limitation under ambient
1077 CO_2, due to the high P deficiency at these sites which is representative of Central Amazon and tropical P limited
1078 sites, and elevated CO_2 resulted in a further subsequent decrease in the land C sink capacity relative to the
1079 model without P limitation. While our study is a step toward the full nutrient cycling representation in ESMs, it
1080 can also help the empirical community to test different hypotheses (i.e., dynamic allocation and stoichiometry)
1081 and generate targeted experimental measurements (Medlyn *et al.*, 2015).
1082
1083 *Code availability*
1084 The modified version of JULES vn5_5 and the P extension developed for this paper are freely available on Met
1085 Office Science Repository Service:
1086 https://code.metoffice.gov.uk/svn/jules/main/branches/dev/mahdinakhavali/vn5.5_JULES_PM_NAKHAVALI/
1087 after registration (http://jules-lsm.github.io/access_req/JULES_access.html) and completion of software license
1088 form. Codes for compiling model available at: (https://doi.org/10.5281/zenodo.5711160). Simulations were
1089 conducted using two sets of model configurations (namelists): ambient CO_2 condition
1090 (https://doi.org/10.5281/zenodo.5711144) and elevated CO_2 condition
1091 (https://doi.org/10.5281/zenodo.5711150).
1092
1093 *Data availability*
1094 The model outputs related to the results in this paper are provided on Zenodo repository
1095 (https://doi.org/10.5281/zenodo.5710898). All the R scripts used for processing the model outputs and
1096 producing results in form of table or figures are provided on Zenodo repository
1097 (https://doi.org/10.5281/zenodo.5710896).

1097 *Author contributions.* MAN, LMM, SS, SEC, CAQ, AJW, IAP, KMA and DBC developed the model, per-
1098 formed simulations and analysis. CAQ, FVC, RP, LFL, KMA, GR, LS, ACMM, JSR, RA and JLC provided the
1099 measurements for the model parasitisation and evaluation. MAN, LMM, SS, IAP, SEC, FVC, RP, LFL, KMA
1100 and DBC contributed in writing the manuscript.
1101
1102 *Competing interests.* The authors declare no competing interests
1103
1104 *Acknowledgment*s. This work and its contributors (MAN, LMM, KMA and IPH) were supported by the UK
1105 Natural Environment Research Council (NERC) grant no. NE/LE007223/1. MAN, LMM, SS, IPH were also
1106 supported by the Newton Fund through the Met Office Climate Science for Service Partnership Brazil (CSSP
1107 Brazil). LMM acknowledges support from the Natural Environment Research Council, grant NEC05816 LTS-
1108 M-UKESM. LFL was also supported by AmazonFACE programme (CAPES) and the National Institute of
1109 Amazonian Research, grant no: 88887.154643/2017-00. The authors acknowledge contributions from Celso
1110 Von Randow towards data curation of the meteorological forcing used in this study and Daniel Goll for
1111 modelling insight. We would like to thank Alessandro C. de Araújo and the Large-Scale Biosphere-Atmosphere
1112 Program (LBA), coordinated by the National Institute for Amazon Researches (INPA), for the use and
1113 availability of data.

References:

Aerts, R. and Chapin, F. S. (1999) 'The Mineral Nutrition of Wild Plants Revisited: A Re-evaluation of Processes and Patterns', *Advances in Ecological Research*, 30(C), pp. 1–67. doi: 10.1016/S0065-2504(08)60016-1.

Anav, A. *et al.* (2013) 'Evaluating the land and ocean components of the global carbon cycle in the CMIP5 earth system models', *Journal of Climate*, 26(18), pp. 6801–6843. doi: 10.1175/JCLI-D-12-00417.1.

Aragão, L. E. O. C. *et al.* (2009) 'Above- and below-ground net primary productivity across ten Amazonian forests on contrasting soils', *Biogeosciences Discussions*, 6(1), pp. 2441–2488. doi: 10.5194/bgd-6-2441-2009.

Aragõ, L. E. O. C. *et al.* (2009) 'Above- and below-ground net primary productivity across ten Amazonian forests on contrasting soils', *Biogeosciences*, 6(12), pp. 2759–2778. doi: 10.5194/bg-6-2759-2009.

Araújo, A. C. *et al.* (2002) 'Comparative measurements of carbon dioxide fluxes from two nearby towers in a central Amazonian rainforest: The Manaus LBA site', *Journal of Geophysical Research*, 107(D20), p. 8090. doi: 10.1029/2001JD000676.

Argles, A. P. K. *et al.* (2020) 'Robust Ecosystem Demography (RED version 1.0): A parsimonious approach to modelling vegetation dynamics in Earth system models', *Geoscientific Model Development*, 13(9), pp. 4067–4089. doi: 10.5194/gmd-13-4067-2020.

Arora, V. K. *et al.* (2020) 'Carbon–concentration and carbon–climate feedbacks in CMIP6 models and their comparison to CMIP5 models', *Biogeosciences*, 17(16), pp. 4173–4222. doi: 10.5194/bg-17-4173-2020.

Baig, S. *et al.* (2015) 'Does the growth response of woody plants to elevated CO2 increase with temperature? A model-oriented meta-analysis', *Global Change Biology*, 21(12), pp. 4303–4319. doi: 10.1111/gcb.12962.

Baker, T. R. *et al.* (2004) 'Variation in wood density determines spatial patterns in Amazonian forest biomass', *Global Change Biology*, 10(5), pp. 545–562. doi: 10.1111/j.1365-2486.2004.00751.x.

Bentsen, M. *et al.* (2013) 'The Norwegian Earth System Model, NorESM1-M – Part 1: Description and basic evaluation of the physical climate', *Geoscientific Model Development*, 6(3), pp. 687–720. doi: 10.5194/gmd-6-687-2013.

Best, M. J. *et al.* (2011) 'The Joint UK Land Environment Simulator (JULES), model description – Part 1: Carbon fluxes and vegetation dynamics', *Geoscientific Model Development*, 4(3), pp. 701–722. doi: 10.5194/gmd-4-701-2011.

Bradford, M. A. and Crowther, T. W. (2013) 'Carbon use efficiency and storage in terrestrial ecosystems', *New Phytologist*, 199(1), pp. 7–9. doi: 10.1111/nph.12334.

Brienen, R. J. W. *et al.* (2015) 'Long-term decline of the Amazon carbon sink', *Nature*, 519(7543), pp. 344–348. doi: 10.1038/nature14283.

Bruijnzeel, L. A. (1991) 'Nutrient input—output budgets of tropical forest ecosystems: A review', *Journal of Tropical Ecology*, 7(1), pp. 1–24. doi: 10.1017/S0266467400005010.

Burke, E. J., Chadburn, S. E. and Ekici, A. (2017) 'A vertical representation of soil carbon in the JULES land surface scheme (vn4.3-permafrost) with a focus on permafrost regions', *Geoscientific Model Development*, 10(2), pp. 959–975. doi: 10.5194/gmd-10-959-2017.

Castanho, A. D. A. *et al.* (2013) 'Improving simulated Amazon forest biomass and productivity by including spatial variation in biophysical parameters', *Biogeosciences*, 10(4), pp. 2255–2272. doi: 10.5194/bg-10-2255-2013.

Chapin, F. S. *et al.* (2011) *Principles of Terrestrial Ecosystem Ecology*. Springer New York (Biomedical and Life Sciences). Available at: https://books.google.co.uk/books?id=68nFNpceRmIC.

Chave, J. *et al.* (2003) 'Spatial and temporal variation of biomass in a tropical forest: Results from a large census plot in Panama', *Journal of Ecology*, 91(2), pp. 240–252. doi: 10.1046/j.1365-2745.2003.00757.x.

Chave, J. *et al.* (2014) 'Improved allometric models to estimate the aboveground biomass of tropical trees', *Global Change Biology*, 20(10), pp. 3177–3190. doi: 10.1111/gcb.12629.

Clark, D. B. *et al.* (2011) 'The Joint UK Land Environment Simulator (JULES), model description – Part 2: Carbon fluxes and vegetation dynamics', *Geoscientific Model Development*, 4(3), pp. 701–722. doi: 10.5194/gmd-4-701-2011.

Collatz, G. J. *et al.* (1991) 'Physiological and environmental regulation of stomatal conductance, photosynthesis and transpiration: a model that includes a laminar boundary layer', *Agricultural and Forest Meteorology*, 54(2–4), pp. 107–136. doi: 10.1016/0168-1923(91)90002-8.

Collatz, G., Ribas-Carbo, M. and Berry, J. (1992) 'Coupled Photosynthesis-Stomatal Conductance Model for Leaves of C4 Plants', *Functional Plant Biology*, 19(5), p. 519. doi: 10.1071/pp9920519.

Comins, H. N. and McMurtrie, R. E. (1993) 'Long-Term Response of Nutrient-Limited Forests to CO"2 Enrichment; Equilibrium Behavior of Plant-Soil Models', *Ecological Applications*, 3(4), pp. 666–681. doi: 10.2307/1942099.

Costa, M. G. *et al.* (2016) 'Labile and Non-Labile Fractions of Phosphorus and Its Transformations in Soil under Eucalyptus', pp. 1–15. doi: 10.3390/f7010015.

Davidson, E. A. *et al.* (2004) 'Nitrogen and phosphorus limitation of biomass growth in a tropical secondary forest', *Ecological Applications*, 14(4 SUPPL.), pp. 150–163. doi: 10.1890/01-6006.

DeLuca, T. H., Keeney, D. R. and McCarty, G. W. (1992) 'Effect of freeze-thaw-events on mineralization of soil nitrogen', *Biol. Fertil. Soils*, 14, pp. 116–120. doi: 10.1007/BF00336260.

Dieter, D., Elsenbeer, H. and Turner, B. L. (2010) 'Phosphorus fractionation in lowland tropical rainforest soils in central Panama.', *Catena*, 82(2), pp. 118–125. doi: 10.1016/j.catena.2010.05.010.

Ellsworth, D. S. *et al.* (2017) 'Elevated CO2 does not increase eucalypt forest productivity on a low-phosphorus soil', *Nature Climate Change*, 7(4), pp. 279–282. doi: 10.1038/nclimate3235.

Elser, J. J. *et al.* (2007) 'Global analysis of nitrogen and phosphorus limitation of primary producers in freshwater, marine and terrestrial ecosystems', *Ecology Letters*, 10(12), pp. 1135–1142. doi: 10.1111/j.1461-0248.2007.01113.x.

Fernández-Martínez, M. *et al.* (2019) 'Global trends in carbon sinks and their relationships with CO2 and temperature', *Nature Climate Change*, 9(1), pp. 73–79. doi: 10.1038/s41558-018-0367-7.

Fleischer, K. *et al.* (2019) 'Amazon forest response to CO2 fertilization dependent on plant phosphorus acquisition', *Nature Geoscience*. doi: 10.1038/s41561-019-0404-9.

Friedlingstein, P. *et al.* (2006) 'Climate-carbon cycle feedback analysis: Results from the C4MIP model intercomparison', *Journal of Climate*, 19(14), pp. 3337–3353. doi: 10.1175/JCLI3800.1.

Friedlingstein, P. *et al.* (2019) 'Comment on "The global tree restoration potential"', *Science*. doi: 10.1126/science.aay8060.

Fyllas, N. M. *et al.* (2009) 'Basin-wide variations in foliar properties of Amazonian forest: phylogeny, soils and climate', *Biogeosciences*, 6(11), pp. 2677–2708. doi: 10.5194/bg-6-2677-2009.

Gentile, R. *et al.* (2012) 'Effects of long-term exposure to enriched CO2 on the nutrient-supplying capacity of a grassland soil', *Biology and Fertility of Soils*, 48(3), pp. 357–362. doi: http://dx.doi.org/10.1007/s00374-011-0616-7.

Goll, D. S. *et al.* (2017) 'A representation of the phosphorus cycle for ORCHIDEE (revision 4520)', *Geoscientific Model Development*, 10(10), pp. 3745–3770. doi: 10.5194/gmd-10-3745-2017.

Gross, A. *et al.* (2021) 'Direct foliar uptake of phosphorus from desert dust', *New Phytologist*, 230(6), pp. 2213–2225. doi: 10.1111/nph.17344.

Harper, A. B. *et al.* (2016) 'Improved representation of plant functional types and physiology in the Joint UK Land Environment Simulator (JULES v4.2) using plant trait information', *Geoscientific Model Development*, 9(7), pp. 2415–2440. doi: 10.5194/gmd-9-2415-2016.

Harris, I. *et al.* (2014) 'Updated high-resolution grids of monthly climatic observations - the CRU TS3.10 Dataset', *International Journal of Climatology*, 34(3), pp. 623–642. doi: 10.1002/joc.3711.

Hatfield, J. L. and Dold, C. (2019) 'Water-use efficiency: Advances and challenges in a changing climate', *Frontiers in Plant Science*, 10(February), pp. 1–14. doi: 10.3389/fpls.2019.00103.

Haverd, V. *et al.* (2018) 'A new version of the CABLE land surface model (Subversion revision r4601) incorporating land use and land cover change, woody vegetation demography, and a novel optimisation-based approach to plant coordination of photosynthesis', *Geoscientific Model Development*, 11(7), pp. 2995–3026. doi: 10.5194/gmd-11-2995-2018.

He, M. and Dijkstra, F. A. (2014) 'Drought effect on plant nitrogen and phosphorus: A meta-analysis', *New Phytologist*, 204(4), pp. 924–931. doi: 10.1111/nph.12952.

Hedley, M. J., Stewart, J. W. B. and Chauhan, B. S. (1982) 'Changes in Inorganic and Organic Soil Phosphorus Fractions Induced by Cultivation Practices and by Laboratory Incubations', *Soil Science Society of America Journal*, 46(5), pp. 970–976. doi: https://doi.org/10.2136/sssaj1982.03615995004600050017x.

Herbert, D. A., Williams, M. and Rastetter, E. B. (2003) 'A model analysis of N and P limitation on carbon accumulation in Amazonian secondary forest after alternate land-use abandonment', *Biogeochemistry*, 65(1), pp. 121–150. doi: 10.1023/A:1026020210887.

Hou, E. *et al.* (2019) 'Quantifying Soil Phosphorus Dynamics: A Data Assimilation Approach', *Journal of Geophysical Research: Biogeosciences*, 124(7), pp. 2159–2173. doi: 10.1029/2018JG004903.

Hou, E. *et al.* (2020) 'Global meta-analysis shows pervasive phosphorus limitation of aboveground plant production in natural terrestrial ecosystems', *Nature Communications*, 11(1), pp. 1–9. doi: 10.1038/s41467-020-14492-w.

Hubau, W. *et al.* (2020) 'Asynchronous carbon sink saturation in African and Amazonian tropical forests', *Nature*, 579(7797), pp. 80–87. doi: 10.1038/s41586-020-2035-0.

Hungate, B. a *et al.* (2003) 'Nitrogen and Climate Change', *Science*, 302(November), pp. 1512–1513.

Jenkinson, D. S. *et al.* (1990) 'The turnover of organic carbon and nitrogen in soil', *The Royal Society*, 329(1255). doi: https://doi.org/10.1098/rstb.1990.0177.

Jenkinson, D. S. and Coleman, K. (2008) 'The turnover of organic carbon in subsoils. Part 2. Modelling carbon turnover', *European Journal of Soil Science*, 59(2), pp. 400–413. doi: 10.1111/j.1365-2389.2008.01026.x.

Ji, D. *et al.* (2014) 'Description and basic evaluation of Beijing Normal University Earth System Model (BNU-

ESM) version 1', *Geoscientific Model Development*, 7(5), pp. 2039–2064. doi: 10.5194/gmd-7-2039-2014.

Jiang, M. *et al.* (2019) 'Towards a more physiological representation of vegetation phosphorus processes in land surface models', *New Phytologist*, 222(3), pp. 1223–1229. doi: 10.1111/nph.15688.

Jiang, M. *et al.* (2020) 'The fate of carbon in a mature forest under carbon dioxide enrichment', *Nature*, 580(7802), pp. 227–231. doi: 10.1038/s41586-020-2128-9.

Jiménez, E. M. *et al.* (2009) 'Fine root dynamics for forests on contrasting soils in the Colombian Amazon', *Biogeosciences*, 6(12), pp. 2809–2827. doi: 10.5194/bg-6-2809-2009.

Johnson, M. O. *et al.* (2016) 'Variation in stem mortality rates determines patterns of above-ground biomass in Amazonian forests: implications for dynamic global vegetation models', *Global Change Biology*, 22(12), pp. 3996–4013. doi: 10.1111/gcb.13315.

Jones, S. *et al.* (2020) 'The impact of a simple representation of non-structural carbohydrates on the simulated response of tropical forests to drought', *Biogeosciences*, 17(13), pp. 3589–3612. doi: 10.5194/bg-17-3589-2020.

Kattge, J. *et al.* (2009) 'Quantifying photosynthetic capacity and its relationship to leaf nitrogen content for global-scale terrestrial biosphere models', *Global Change Biology*, 15(4), pp. 976–991. doi: https://doi.org/10.1111/j.1365-2486.2008.01744.x.

Keller, M. *et al.* (2004) 'Ecological research in the Large-scale Biosphere-Atmosphere Experiment in Amazonia: Early results', *Ecological Applications*, 14(4 SUPPL.), pp. 3–16. doi: 10.1890/03-6003.

Klein, T. *et al.* (2016) 'Growth and carbon relations of mature Picea abies trees under 5 years of free-air CO2 enrichment', *Journal of Ecology*, 104(6), pp. 1720–1733. doi: 10.1111/1365-2745.12621.

Koch, A., Hubau, W. and Lewis, S. L. (2021) 'Earth System Models Are Not Capturing Present-Day Tropical Forest Carbon Dynamics', *Earth's Future*, 9(5), pp. 1–19. doi: 10.1029/2020EF001874.

Körner, C. *et al.* (2005) 'Ecology: Carbon flux and growth in mature deciduous forest trees exposed to elevated CO2', *Science*, 309(5739), pp. 1360–1362. doi: 10.1126/science.1113977.

Van Langenhove, L. *et al.* (2020) 'Atmospheric deposition of elements and its relevance for nutrient budgets of tropical forests', *Biogeochemistry*, 149(2), pp. 175–193. doi: 10.1007/s10533-020-00673-8.

Lapola, D. M. and Norby, R. (2014) 'Assessing the effects of increased atmospheric CO 2 on the ecology and resilience of the Amazon forest', *Science plan et implementation strategy*, AMAZON FAC.

LeBauer, D. and Treseder, K. (2008) 'Nitrogen Limitation of Net Primary Productivity', *Ecology*, 89(2), pp. 371–379.

Lloyd, J. *et al.* (2001) 'Should Phosphorus Availability Be Constraining Moist Tropical Forest Responses to Increasing CO2 Concentrations?', in *Global Biogeochemical Cycles in the Climate System*. Elsevier, pp. 95–114. doi: 10.1016/B978-012631260-7/50010-8.

Long, M. C. *et al.* (2013) 'Twentieth-century oceanic carbon uptake and storage in CESM1(BGC)', *Journal of Climate*, 26(18), pp. 6775–6800. doi: 10.1175/JCLI-D-12-00184.1.

De Lucia, E. H. *et al.* (2007) 'Forest carbon use efficiency: Is respiration a constant fraction of gross primary production?', *Global Change Biology*, 13(6), pp. 1157–1167. doi: 10.1111/j.1365-2486.2007.01365.x.

Lugli, L. F. (2013) *Estoque de nutrientes na serrapilheira fina e grossa em função de fatores edáficos em florestas do Amazonas, Brasil*. Instituto Nacional de Pesquisas da Amazônia - INPA. Available at: https://repositorio.inpa.gov.br/handle/1/5028.

Lugli, L. F. *et al.* (2020) 'Multiple phosphorus acquisition strategies adopted by fine roots in low-fertility soils in Central Amazonia', *Plant and Soil*, 450(1–2), pp. 49–63. doi: 10.1007/s11104-019-03963-9.

Lugli, L. F. *et al.* (2021) 'Rapid responses of root traits and productivity to phosphorus and cation additions in a tropical lowland forest in Amazonia', *New Phytologist*, 230(1), pp. 116–128. doi: 10.1111/nph.17154.

Luo, Y. *et al.* (2004) 'Progressive nitrogen limitation of ecosystem responses to rising atmospheric carbon dioxide', *BioScience*, 54(8), pp. 731–739. doi: 10.1641/0006-3568(2004)054[0731:PNLOER]2.0.CO;2.

Malhi, Y. *et al.* (2004) 'The above-ground coarse wood productivity of 104 Neotropical forest plots', *Global Change Biology*, 10(5), pp. 563–591. doi: 10.1111/j.1529-8817.2003.00778.x.

Malhi, Y. *et al.* (2006) 'The regional variation of aboveground live biomass in old-growth Amazonian forests', *Global Change Biology*, 12(7), pp. 1107–1138. doi: 10.1111/j.1365-2486.2006.01120.x.

Malhi, Y. *et al.* (2009) 'Comprehensive assessment of carbon productivity, allocation and storage in three Amazonian forests', *Global Change Biology*, 15(5), pp. 1255–1274. doi: 10.1111/j.1365-2486.2008.01780.x.

Malhi, Y. (2012) 'The productivity, metabolism and carbon cycle of tropical forest vegetation', *Journal of Ecology*, 100(1), pp. 65–75. doi: 10.1111/j.1365-2745.2011.01916.x.

Malhi, Y., Doughty, C. and Galbraith, D. (2011) 'The allocation of ecosystem net primary productivity in tropical forests', *Philosophical Transactions of the Royal Society B: Biological Sciences*, 366(1582), pp. 3225–3245. doi: 10.1098/rstb.2011.0062.

Martins, N. P. *et al.* (2021) 'Fine roots stimulate nutrient release during early stages of leaf litter decomposition in a Central Amazon rainforest', *Plant and Soil*, 469(1–2), pp. 287–303. doi: 10.1007/s11104-021-05148-9.

Medlyn, B. E. *et al.* (2015) 'Using ecosystem experiments to improve vegetation models', *Nature Climate Change*, 5(6), pp. 528–534. doi: 10.1038/nclimate2621.

Medlyn, B. E. *et al.* (2016) 'Using models to guide field experiments: a priori predictions for the CO2 response of a nutrient- and water-limited native Eucalypt woodland', *Global Change Biology*, 22(8), pp. 2834–2851. doi: 10.1111/gcb.13268.

Mercado, L. M. *et al.* (2011) 'Variations in Amazon forest productivity correlated with foliar nutrients and modelled rates of photosynthetic carbon supply', *Philosophical Transactions of the Royal Society B: Biological Sciences*, 366(1582), pp. 3316–3329. doi: 10.1098/rstb.2011.0045.

Mirabello, M. J. *et al.* (2013) 'Soil phosphorus responses to chronic nutrient fertilisation and seasonal drought in a humid lowland forest, Panama', *Soil Research*, 51(3), pp. 215–221. doi: 10.1071/SR12188.

Mitchard, E. T. A. (2018) 'The tropical forest carbon cycle and climate change', *Nature*, 559(7715), pp. 527–534. doi: 10.1038/s41586-018-0300-2.

Nachtergaele, F. *et al.* (2010) 'The Harmonized World Soil Database', *Proceedings of the 19th World Congress of Soil Science, Soil Solutions for a Changing World, Brisbane, Australia, 1-6 August 2010*, pp. 34–37. doi: 3123.

Neff, J. C., Hobbie, S. E. and Vitousek, P. M. (2000) 'Nutrient and mineralogical control on dissolved organic C, N and P fluxes and stoichiometry in Hawaiian soils', *Biogeochemistry*, 51(3), pp. 283–302. doi: 10.1023/A:1006414517212.

Norby, R. J. *et al.* (2016) 'Model–data synthesis for the next generation of forest free-air <scp>CO</scp> 2 enrichment (<scp>FACE</scp>) experiments', *New Phytologist*, 209(1), pp. 17–28. doi: 10.1111/nph.13593.

Nordin, A., Högberg, P. and Näsholm, T. (2001) 'Soil nitrogen form and plant nitrogen uptake along a boreal forest productivity gradient', *Oecologia*, 129(1), pp. 125–132. doi: 10.1007/s004420100698.

Pan, Y. *et al.* (2011) 'A Large and Persistent Carbon Sink in the World's Forests', *Science*, 333(6045), pp. 988–993. doi: 10.1126/science.1201609.

Perakis, S. S. and Hedin, L. O. (2002) 'Nitrogen loss from unpolluted South American forests mainly via dissolved organic compounds', *Nature*, 415(6870), pp. 416–419. doi: 10.1038/415416a.

Phillips, O. L. *et al.* (2004) 'Pattern and process in Amazon tree turnover, 1976-2001', *Philosophical Transactions of the Royal Society B: Biological Sciences*, 359(1443), pp. 381–407. doi: 10.1098/rstb.2003.1438.

Phillips, O. L. *et al.* (2017) 'Carbon uptake by mature Amazon forests has mitigated Amazon nations' carbon emissions', *Carbon Balance and Management*, 12(1), pp. 1–9. doi: 10.1186/s13021-016-0069-2.

Pyle, E. H. *et al.* (2009) 'Dynamics of carbon, biomass, and structure in two Amazonian forests', *Journal of Geophysical Research: Biogeosciences*, 114(1), pp. 1–20. doi: 10.1029/2007JG000592.

Quesada, C. A. *et al.* (2010) 'Variations in chemical and physical properties of Amazon forest soils in relation to their genesis', *Biogeosciences*, 7(5), pp. 1515–1541. doi: 10.5194/bg-7-1515-2010.

Quesada, C. A. *et al.* (2011) 'Soils of Amazonia with particular reference to the RAINFOR sites', *Biogeosciences*, 8(6), pp. 1415–1440. doi: 10.5194/bg-8-1415-2011.

Quesada, C. A. *et al.* (2012) 'Basin-wide variations in Amazon forest structure and function are mediated by both soils and climate', *Biogeosciences*, 9(6), pp. 2203–2246. doi: 10.5194/bg-9-2203-2012.

Reed, S. C., Yang, X. and Thornton, P. E. (2015) 'Incorporating phosphorus cycling into global modeling efforts: A worthwhile, tractable endeavor', *New Phytologist*, 208(2), pp. 324–329. doi: 10.1111/nph.13521.

Ryan, M. G. (2013) 'Three decades of research at Flakaliden advancing whole-tree physiology, forest ecosystem and global change research', *Tree Physiology*, 33(11), pp. 1123–1131. doi: 10.1093/treephys/tpt100.

Sampaio, G. *et al.* (2021) 'CO2physiological effect can cause rainfall decrease as strong as large-scale deforestation in the Amazon', *Biogeosciences*, 18(8), pp. 2511–2525. doi: 10.5194/bg-18-2511-2021.

Sanchez, P. A. (1977) 'Properties and Management of Soils in the Tropics', *Soil Science*, 124(3). Available at: https://journals.lww.com/soilsci/Fulltext/1977/09000/Properties_and_Management_of_Soils_in_the_Tropics.12.aspx.

Sardans, J., Rivas-Ubach, A. and Peñuelas, J. (2012) 'The C:N:P stoichiometry of organisms and ecosystems in a changing world: A review and perspectives', *Perspectives in Plant Ecology, Evolution and Systematics*, 14(1), pp. 33–47. doi: 10.1016/j.ppees.2011.08.002.

Schimel, D., Stephens, B. B. and Fisher, J. B. (2015) 'Effect of increasing CO2 on the terrestrial carbon cycle', *Proceedings of the National Academy of Sciences of the United States of America*, 112(2), pp. 436–441. doi: 10.1073/pnas.1407302112.

Shen, J. *et al.* (2011) 'Phosphorus dynamics: From soil to plant', *Plant Physiology*, 156(3), pp. 997–1005. doi: 10.1104/pp.111.175232.

Sitch, S. *et al.* (2008) 'Evaluation of the terrestrial carbon cycle, future plant geography and climate-carbon cycle feedbacks using five Dynamic Global Vegetation Models (DGVMs)', *Global Change Biology*, 14(9), pp. 2015–2039. doi: 10.1111/j.1365-2486.2008.01626.x.

Stephenson, N. L. and Van Mantgem, P. J. (2005) 'Forest turnover rates follow global and regional patterns of productivity', *Ecology Letters*, 8(5), pp. 524–531. doi: 10.1111/j.1461-0248.2005.00746.x.

Sun, Y. *et al.* (2021) 'Global evaluation of the nutrient-enabled version of the land surface model ORCHIDEE-CNP v1.2 (r5986)', *Geoscientific Model Development*, 14(4), pp. 1987–2010. doi: 10.5194/gmd-14-1987-2021.

1354   Turner, B. L. *et al.* (2015) 'Seasonal changes in soil organic matter after a decade of nutrient addition in a
1355   lowland tropical forest', *Biogeochemistry*, 123(1–2), pp. 221–235. doi: 10.1007/s10533-014-0064-1.
1356   Turner, B. L. and Condron, L. M. (2013) 'Pedogenesis, nutrient dynamics, and ecosystem development: the
1357   legacy of T.W. Walker and J.K. Syers', *Plant and Soil*, 367(1–2), pp. 1–10. doi: 10.1007/s11104-013-1750-9.
1358   Vicca, S. *et al.* (2012a) 'Fertile forests produce biomass more efficiently', *Ecology Letters*, 15(6), pp. 520–526.
1359   doi: 10.1111/j.1461-0248.2012.01775.x.
1360   Vicca, S. *et al.* (2012b) 'Fertile forests produce biomass more efficiently', *Ecology Letters*, 15(6), pp. 520–526.
1361   doi: 10.1111/j.1461-0248.2012.01775.x.
1362   Vitousek, P. M. *et al.* (1997) 'Human Domination of Earth Ecosystems', *Science*, 278(5335), p. 21. Available
1363   at: http://www.cheric.org/research/tech/periodicals/view.php?seq=257860.
1364   Vitousek, P. M. (2004) *Nutrient Cycling and Limitation: Hawai'i as a Model System*. Princeton University Press
1365   (Princeton Environmental Institute series). Available at:
1366   https://books.google.com.fj/books?id=6EmAtAEACAAJ.
1367   Vitousek, P. M. *et al.* (2010) 'Terrestrial phosphorus limitation: Mechanisms, implications, and nitrogen-
1368   phosphorus interactions', *Ecological Applications*, 20(1), pp. 5–15. doi: 10.1890/08-0127.1.
1369   Vitousek, P. M. and Howarth, R. W. (1991) 'Nitrogen limitation on land and in the sea: How can it occur?',
1370   *Biogeochemistry*, 13(2), pp. 87–115. doi: 10.1007/BF00002772.
1371   Walker, A. P. *et al.* (2021) 'Integrating the evidence for a terrestrial carbon sink caused by increasing
1372   atmospheric CO2', *New Phytologist*, 229(5), pp. 2413–2445. doi: 10.1111/nph.16866.
1373   Walker, T. W. and Syers, J. K. (1976) 'The fate of phosphorus during pedogenesis', *Geoderma*, 15(1), pp. 1–19.
1374   doi: 10.1016/0016-7061(76)90066-5.
1375   Wang, Y. P., Houlton, B. Z. and Field, C. B. (2007) 'A model of biogeochemical cycles of carbon, nitrogen, and
1376   phosphorus including symbiotic nitrogen fixation and phosphatase production', *Global Biogeochemical Cycles*,
1377   21(1), pp. 1–15. doi: 10.1029/2006GB002797.
1378   Wang, Y. P., Law, R. M. and Pak, B. (2010) 'A global model of carbon, nitrogen and phosphorus cycles for the
1379   terrestrial biosphere', *Biogeosciences*, 7(7), pp. 2261–2282. doi: 10.5194/bg-7-2261-2010.
1380   Went, F. W. and Stark, N. (1968) 'Mycorrhiza', *BioScience*, 18(11), pp. 1035–1039. doi: 10.2307/1294552.
1381   Wiltshire, A. J. *et al.* (2020) 'JULES-CN : a coupled terrestrial Carbon-Nitrogen Scheme (JULES vn5 . 1)',
1382   (July), pp. 1–40.
1383   Wiltshire, A. J. *et al.* (2021) 'Jules-cn: A coupled terrestrial carbon-nitrogen scheme (jules vn5.1)',
1384   *Geoscientific Model Development*, 14(4), pp. 2161–2186. doi: 10.5194/gmd-14-2161-2021.
1385   Wright, S. J. *et al.* (2011) 'Potassium, phosphorus, or nitrogen limit root allocation, tree growth, or litter
1386   production in a lowland tropical forest', *Ecology*, 92(8), pp. 1616–1625. doi: 10.1890/10-1558.1.
1387   Xiao, J. *et al.* (2013) 'Carbon fluxes, evapotranspiration, and water use efficiency of terrestrial ecosystems in
1388   China', *Agricultural and Forest Meteorology*, 182–183, pp. 76–90. doi: 10.1016/j.agrformet.2013.08.007.
1389   Xu, Z. *et al.* (2016) 'Elevated-CO2 response of stomata and its dependence on environmental factors', *Frontiers
1390   in Plant Science*, 7(MAY2016), pp. 1–15. doi: 10.3389/fpls.2016.00657.
1391   Yang, X. *et al.* (2013) 'The distribution of soil phosphorus for global biogeochemical modeling',
1392   *Biogeosciences*, 10(4), pp. 2525–2537. doi: 10.5194/bg-10-2525-2013.
1393   Yang, X. *et al.* (2014) 'The role of phosphorus dynamics in tropical forests – a modeling study using CLM-
1394   CNP', *Biogeosciences*, 11(6), pp. 1667–1681. doi: 10.5194/bg-11-1667-2014.
1395   Yang, X. and Post, W. M. (2011) 'Phosphorus transformations as a function of pedogenesis: A synthesis of soil
1396   phosphorus data using Hedley fractionation method', *Biogeosciences*, 8(10), pp. 2907–2916. doi: 10.5194/bg-8-
1397   2907-2011.
1398   Zaehle, S. and Dalmonech, D. (2011) 'Carbon-nitrogen interactions on land at global scales: Current
1399   understanding in modelling climate biosphere feedbacks', *Current Opinion in Environmental Sustainability*,
1400   3(5), pp. 311–320. doi: 10.1016/j.cosust.2011.08.008.
1401   Zaehle, S. and Friend, A. D. (2010) 'Carbon and nitrogen cycle dynamics in the O-CN land surface model: 1.
1402   Model description, site-scale evaluation, and sensitivity to parameter estimates', *Global Biogeochemical Cycles*,
1403   24(1), pp. 1–13. doi: 10.1029/2009GB003521.
1404   Zhu, Q. *et al.* (2016) 'Multiple soil nutrient competition between plants, microbes, and mineral surfaces: model
1405   development, parameterization, and example applications in several tropical forests', *Biogeosciences*, 13(1), pp.
1406   341–363. doi: 10.5194/bg-13-341-2016.
1407